Manuscript prepared for Atmos. Chem. Phys.
with version 2015/04/24 7.83 Copernicus papers of the LaTeX class copernicus.cls.
Date: 29 February 2016

Modeling lightning-NO_x chemistry at sub-grid scale in a global chemical transport model

Alicia Gressent[1], Bastien Sauvage[1], Daniel Cariolle[2,3], Mathew Evans[4], Maud Leriche[1], Céline Mari[1], and Valérie Thouret[1]

[1]LA, CNRS, Université de Toulouse, Toulouse, France
[2]Météo France, Toulouse
[3]Centre Européen de Recherche et de Formation Avancée en Calcul Scientifique, CERFACS, Toulouse
[4]The Wolfson Atmospheric Chemistry Laboratories, University of York, UK

Correspondence to: Alicia Gressent (alicia.gressent@aero.obs-mip.fr)

Abstract. For the first time, a plume-in-grid approach is implemented in a chemical transport model (CTM) to parameterize the effects of the non-linear reactions occurring within high concentrated NO_x plumes from lightning NO_x emissions (LNO_x) in the upper troposphere. It is characterized by a set of parameters including the plume lifetime, the effective reaction rate constant related to NO_x-O_3 chemical interactions and the fractions of NO_x conversion into HNO_3 within the plume. Parameter estimates were made using the DSMACC chemical box model, simple plume dispersion simulations and the mesoscale 3-D Meso-NH model. In order to assess the impact of the LNO_x plume approach on the NO_x and O_3 distributions at large scale, simulations for the year 2006 were performed using the GEOS-Chem global model with a horizontal resolution of $2^\circ \times 2.5^\circ$. The implementation of the LNO_x parameterization implies NO_x and O_3 decrease at large scale over the region characterized by a strong lightning activity (up to 25 % and 8 %, respectively, over Central Africa in July) and a relative increase downwind of LNO_x emissions (up to 18 % and 2 % for NO_x and O_3, respectively, in July) are derived. The calculated variability of NO_x and O_3 mixing ratios around the mean value according to the known uncertainties on the parameter estimates is maximum over continental tropical regions with ΔNO_x $[-33.1; +29.7]$ ppt and ΔO_3 $[-1.56; +2.16]$ ppb, in January, and ΔNO_x $[-14.3; +21]$ ppt and ΔO_3 $[-1.18; +1.93]$ ppb, in July, mainly depending on the determination of the diffusion properties of the atmosphere and the initial NO mixing ratio injected by lightning. This approach allows (i) to reproduce a more realistic lightning NO_x chemistry leading to better NO_x and O_3 distributions at the large scale and (ii) focus on other improvements to reduce remaining uncertainties from processes related to NO_x chemistry in CTM.

1 Introduction

Lightning emissions are one of the most important sources of nitrogen oxides ($NO_x \equiv NO + NO_2$) in the upper troposphere (WMO, 1999; Hudman et al., 2007). Lightning primarily produce NO and

may also induce a negligible quantity of NO_2 with a ratio NO_2/NO_x of 0.5 to 0.1 (Franzblau, 1991; Stark et al., 1996). NO_x emitted by lightning (LNO_x) impact the tropospheric ozone burden (Stockwell et al., 1999; Hauglustaine et al., 2001; Grewe, 2007), and the hydroxyl-radical (OH) concentrations influencing the oxidizing capacity of the atmosphere (Labrador et al., 2004; Banerjee et al., 2014). Most NO_x produced by lightning is detrained into the free and upper troposphere, where ozone production efficiencies (OPE) per unit NO_x emitted are 4 to 20 higher than at the surface (Sauvage et al., 2007a; Martin et al., 2007), and therefore lightning exerts a disproportionately stronger effect on photochemistry than surface emissions (Pickering et al., 1990; Hauglustaine et al., 1994; Zhang et al., 2003; Choi et al., 2009). The longer NO_x lifetime in the upper troposphere (1-2 weeks) allows the long-range transport of LNO_x through the large circulation patterns (Hemispheric Transport of Air Pollution, HTAP report, 2010: http://www.htap.org/).

Although the importance of the LNO_x emissions on the upper tropospheric chemistry is well known, it remains highly uncertain with a best estimate of 2-8 $TgN{\cdot}yr^{-1}$ (Schumann and Huntrieser, 2007). Lightning NO_x emissions are associated with deep convection (horizontal scale ~ 10 km) and correspond to the "sub-grid" in global chemical transport models (horizontal resolution $\sim 100s$ km). Therefore, lightning NO_x production must be parameterized for inclusion into a large scale model. Global models commonly used convection proxies such as the cloud-top-height (Price and Rind, 1992) and the updraft intensity to estimate the lightning flashes. Flashes simulated by CTMs are commonly constrained by satellite observations (Sauvage et al., 2007b; Murray et al., 2012) from the space-borne Lightning Imaging Sensor (LIS) on TRMM and the Optical Transient Detector (OTD) (Christian et al., 2003; Tost et al., 2007). The lightning NO_x emissions are then redistributed according to a vertical profile generally a reverse "C-Shape" profile (Ott et al., 2010) a priori defined depending on season, latitude and continent/ocean location. Also, corrections on the calculations of lightning NO_x emissions using satellite observations (SCIAMACHY, Martin et al. (2007)) and in-situ measurements (INTEX-NA, Hudman et al. (2007)) are usually applied.

Despite the necessity of including lightning NO_x emissions in global models, the small scale nature of the flashes and the non-linear chemistry (Lin et al., 1988) of the atmosphere will lead to biases on the large scale with instantaneous dilution of gases in the large grid box volume. It seems likely that this will lead to an overestimate of the OPE and an underestimate of the nitric acid (HNO_3) production. For instance, by forcing NO_x concentration in GEOS-Chem grid box over Southeast Asia to represent the measured lightning plumes, Cooper et al. (2014) estimated a ratio for O_3 to HNO_3 produced leading to a 15 mol/mol OPE in lightning plumes, that reinforces the fact that instantaneous dilution in global model implies issues in sub-grid chemistry.

In this work, a more realistic lightning NO_x chemistry as well as a plume parameterization is implemented into a global chemical transport model (CTM) allowing reproducing more accurately

the NO_x and O_3 distributions at large scale. The plume approach used in this study was previously developed by Cariole et al. (2009) for aircraft NO_x emissions in the LMDz-INCA and MOBIDIC models and also implemented to deal with the ship NO_x emissions (Huszar et al., 2010). This approach avoids the double count in the CTM calculation of the emitted NO_x, first instantaneously diluted into the point grid and secondly as the plume form. In addition, the plume parameterization is the first that considers the NO_x from lightning as a plume with the transport of the related non-linear chemistry effects. NO_x from lightning emissions are emitted in the upper troposphere characterized by strong winds allowing the large scale transport of trace species. Thus, it is relevant to consider a plume growth from lightning emissions, which could be diluted long time after the initial lightning pulse, downwind of emissions. Consequently, the plume parameterization previously developed for aircraft exhausts has been adjusted to LNO_x emissions and implemented into the GEOS-Chem global chemical transport model.

Section 2 gives a description of the GEOS-Chem model in which the plume-in-grid parameterization is implemented and the models which are used to evaluate the diffusion properties of the atmosphere and to determine parameters characterizing the physics and chemistry of the lightning NO_x plume. A concise description of the plume approach is then presented in section 3 followed by a detailed explanation of the determination of parameters related to LNO_x emissions. Section 4 summarizes the results of the simulations performed with GEOS-Chem and finally these results and the sensitivity on NO_x and O_3 variations of the parameterization are discussed in section 5.

2 Models

Three different models are used in this evaluation and are described in this section. GEOS-Chem is used to provide a global framework to assess the impact of lightning NO_x. Meso-NH is used to provide estimates of the plume diffusion timescales and DSMACC is a box model used to assess the non-linear chemistry in the plume.

2.1 The GEOS-Chem chemical transport model

The GEOS-Chem chemical transport model (Bey et al., 2001) is a global 3-D model of atmospheric composition driven by assimilated meteorology from the Goddard Earth Observing System (GEOS-5) of the NASA Global Modeling Assimilation Office (GMAO). The 09-01-01 version (http://wiki.seas.harvard.edu/geos-chem/index.php/GEOS-Chem_v9-01-01) of the CTM has been used in this study. The model transports 43 tracers to describe tropospheric O_3-NO_x-VOC chemistry. The horizontal resolution is $2^\circ \times 2.5^\circ$ and 47 vertical levels are defined from the ground to 80 km altitude. The CTM includes modules for emissions, transport, chemistry, deposition, aerosols

and surface.

The large-scale advection of tracers is performed using the TPCORE advection scheme (Lin and Rood, 1996) corresponding to a semi-lagrangian flux method. Shallow and deep moist convection processes are carried out using the Relaxed Arakawa-Schubert scheme (Moorthi and Suarez, 1991). Mixing in the lower atmospheric layers is represented by a non-local scheme of the planetary boundary layer described by Lin and McElroy (2010). The wet deposition for water-soluble aerosols and for gases follows Liu et al. (2001) and Amos et al. (2012). Aerosol scavenging by ice crystals and cold/mixed precipitation is also reproduced in the model (Wang et al., 2011). The dry deposition is associated to a scheme which calculates bulk surface resistance in series (Wesely, 1989). Photolysis rates are calculated with the Fast-JX code (Bian and Prather, 2002). The atmospheric chemistry is resolved using the SMVGEAR solver (Jacobson and Turco, 1994) with more than 300 species and 785 chemical reactions. Heterogeneous chemical reactions are represented on the surface of aerosols (Bey et al., 2001; Martin et al., 2002). Effects of aerosols on the photolysis rates are based on Martin et al. (2003). Primary NO_x and VOCs (Volatile Organic Compounds) emissions are separated depending on sources. Global anthropogenic emissions are given by the GEIA (Wang et al., 1998) and EGDAR (Olivier, 2005) inventories and regional anthropogenic emissions are overwrite those for the US (NEI05), Canada (CAC), Mexico (BRAVO), Europe (EMEP) and East Asia (Streets et al., 2006; Zhang et al., 2009). Biofuel emissions are provided by EPA and STREETS 2006 inventories (Yevich and Logan, 2003), biomass burning emissions by GFED inventory (van der Werf et al., 2010), and biogenic emissions by the MEGAN model calculations (Guenther et al., 2012). In addition, NO_x from soil emissions are calculated by an algorithm depending on temperature and precipitation (Yienger and Levy, 1995).

In order to calculate the NO_x from lightning, flash rates are first calculated in active deep convection using the Price and Rind Scheme based on the cloud-top-height (Price and Rind, 1992, 1994), then flash rates are adjusted with local scaling factors to match the satellite climatology (Sauvage et al., 2007b; Murray et al., 2012), and the total column emissions are determined using NO_x yields that differ in tropics and northern extratropics. Finally, the total column is distributed vertically using the reverse C-shaped profile from Ott et al. (2010). Note that the base lightning NO_x scheme is described in detail by Murray et al. (2012).

2.2 The Meso-NH model

The Meso-NH model is an atmospheric model developed jointly by the Laboratoire d'Aérologie and by CNRM-GAME (http://mesonh.aero.obs-mip.fr/mesonh51). The model includes a non-hydrostatic and anelastic system of equations (Lafore et al., 1998) and has a complete set of parameterizations allowing to reproduce physical processes such as radiation (Gregory et al., 2000), atmospheric turbu-

lence (Cuxart et al., 1999), convection (Bechtold et al., 2000), microphysics related to warm clouds (Cohard and Pinty, 2000), and atmospheric ice (Pinty and Jabouille, 1999; Lascaux et al., 2006). Meso-NH includes also on-line chemistry (Tulet et al., 2003, 2006). The model deals with large (synoptic) to small (large eddy) scales. In this study, the Mesonh-49 version was used in order to compare the horizontal diffusion coefficient (D_h) estimate within the anvil of thunderstorms from in-situ measurements to a modeling ideal case of a convective cell.

2.3 The DSMACC chemical box model

The Dynamical Simple Model of Atmospheric Chemical Complexity (DSMACC) is a simple box model developed for improving our understanding of the tropospheric chemistry (Emmerson and Evans, 2009). The model is composed of the KPP chemical pre-processor (Damian et al., 2002) to solve differential equations representing the chemical system. The TUV (Tropospheric Ultraviolet and Visible Radiation Model) photolysis scheme is used, which calculates the spectral irradiance, the spectral actinic flux, photodissociation coefficients (J-values) (Madronich and Flocke, 1999), and biologically effective irradiance. The chemical scheme used derives from the Master Chemical Mechanism (MCM, http://mcm.leeds.ac.uk/MCM/), (Jenkin et al., 1997; Saunders et al., 2003), which contains 17000 elementary reactions of 6700 primary, secondary and radical species.

In order to study the chemical interactions that could occur in the undiluted plume fraction, a set of short simulations was carried out with the DSMACC chemical box model as explained in the section 3.2.2.

2.4 The simple plume dispersion model

To model the dispersion of lightning NO_x emissions we use a simple dispersion model similar to the plume model used for aircraft NO_x emissions, except that the plume is supposed to be oriented along a vertical axis. The plume is represented as a cylinder that encompass horizontal diffusion with a constant coefficient D_h (section 3.2.1). This simple model is composed of 30 horizontal circles with spacing increasing progressively from the center axis. The discretization of the diffusion equation is mass conservative.

The chemistry scheme and associated reaction rate constants is adapted from the large-scale chemical model MOCAGE (Teyssèdre et al., 2007). It includes the main reactions involved in the $NO_x - HO_x$ system. Simple plume simulations were performed in order to estimate the physical and chemical characteristics of the plumes related to lightning NO_x emissions.

3 Plume parameterization for lightning NO_x emissions

3.1 General description

The LNO_x plume parameterization is based on a method initially developed by Cariolle et al. (2009) for NO_x emissions related to aircraft exhausts later adapted to ship emissions of NO_x (Huszar et al., 2010). In this approach, the plume effects at sub-grid scale are represented via a fuel tracer, to follow the amount of the emitted species in the plume and an effective reaction rate for the ozone production and nitric acid production/destruction during the plume's dilution into the background (Cariolle et al., 2009; Paoli et al., 2011). The parameterization requires a proper estimation of the characteristic plume lifetime during which the non-linear interactions between species are important and simulated via specific rates of conversion. The approach ensures the mass conservation of species in the model. This is the only method which considers a plume evolution related to the local NO_x emissions allowing the transport of the non-linear effects occurring at smaller scale than the model grid.

3.1.1 Physical plume formulation

Following Cariolle et al. (2009), a passive tracer (from the perspective of the usual model chemistry) is added to the CTM to represent NO_x emitted by lightning. The LNO_x tracer initial mass corresponds to the NO_x mass at the start time of the simulation. Rather than increasing the concentration of NO_x within the CTM, lightning NO_x emissions now increase the concentration of this new passive tracer which is transported in the standard way by advection and turbulence. Plume chemistry is considered to be significant when the mixing ratio of the lightning NO_x tracer is higher than a critical NO_x content, hereafter denoted r_l. Above this value the lightning NO_x tracer is transferred to the normal NO_x tracer at a rate described by a plume lifetime (τ), which is an exponential decay constant. This corresponds to an exchange time scale between the lightning NO_x plume and the background NO_x. The continuity equation related to the tracer evolution is detailed by the equation 1.

$$\frac{\partial \overline{r_{LNO_x}}}{\partial t} + < F_{LNO_x} >= I - \frac{1}{\tau} \cdot \overline{r_{LNO_x}} \tag{1}$$

Where $\overline{r_{LNO_x}}$, is the mixing ratio (in ppb) of the NO_x lightning tracer in the model grid (note that all overlined terms referred to grid average quantities in the CTM), $F_{LNO_x} \equiv \nabla \cdot (\overline{r_{LNO_x}} u) + \nabla \cdot (D_t \nabla \overline{r_{LNO_x}})$ and it corresponds to the flux divergence related to the large-scale transport of the tracer (advection and turbulent diffusion, in $molecules \cdot cm^{-2} \cdot s^{-1}$), I is the injection rate of LNO_x (in s^{-1}) and τ is the plume lifetime (in seconds).

The calculation of τ requires evaluating the mass fraction of the lightning NO_x (M(t)) corresponding to the undiluted fraction of the plume and characterized by a NO_x mixing ratio above the

r_l critical value. In other words, the plume boundary is defined by the critical value r_l depending on the time of day. The NO_x mass, M(t) decreases monotonically to zero until $t = T_l$ for which the tracer mixing ratio is everywhere below the r_l threshold. The plume lifetime is obtained by an exponential function depending on the mass (equations 2 and 3):

$$M(t) = \int_{V_p} \rho \cdot r_p \cdot \mathrm{d}V \tag{2}$$

$$\tau = \int_{t_0=0}^{+\infty} \exp(-t/\tau) \cdot \mathrm{d}t = \frac{1}{M(t_0)} \int_{t_0=0}^{T_l} M(t) \cdot \mathrm{d}t \tag{3}$$

Where V_p is the volume of the plume, ρ is the density of the air, r_p is the NO_x mixing ratio within the plume (in ppb) and T_l is the time for which the mixing ratio r_p is everywhere below the critical value r_l. The calculation of the plume lifetime, by simple plume dispersion simulations, depends on (i) the initial emissions of NO_x by lightning, (ii) the r_l value, and (iii) the dispersion properties of the atmosphere (related to the horizontal diffusion coefficient, D_h) and is detailed on the section 3.2.3.

Note that the mean dispersion properties of the atmosphere were associated with the horizontal diffusion only. The lightning NO_x emissions occur in the convective part of clouds where the vertical diffusion is strong. Therefore, the vertical diffusion coefficient is a determining parameter for the LNO_x distribution in the cloud. As mentioned in section 2.1, the vertical distribution of the LNO_x is a priori calculated from Ott et al. (2010) as a reverse C-shaped profile. The LNO_x plume parameterization is applied a posteriori after that lightning NO_x are vertically prescribed and concerns convective outflow where the NO_x are detrained in the troposphere. In this region of detrainment, the horizontal dispersion may be more efficient than the vertical one as it is discussed in (Cariolle et al., 2009).

3.1.2 Plume chemistry of NO_x, O_3 and HNO_3

Once the lightning NO_x is emitted, it is transferred to model's background NO_x based on the lifetime of the plume (τ). Thus, the continuity equation for the NO_x species emitted in the plume and released to the large scale can be deduced as described by the equation 4.

$$\frac{\partial \overline{r_{NO_x}}}{\partial t} + < F_{NO_x} > = + \frac{1}{\tau} \cdot \overline{r_{LNO_x}} \cdot \alpha_{NO_x} + L_{ss} \tag{4}$$

Where, $\overline{r_{NO_x}}$, is the mixing ratio of NO_x (in ppb) in the model grid, α_{NO_x} is the molecular mass ratio between the air and NO_x species and L_{ss} are the large-scale sources and sinks (in $molecules \cdot cm^{-2} \cdot s^{-1}$) such as natural and anthropogenic emissions, photochemical reaction, mixing, and conversion to reservoir species.

We consider a fairly simple chemistry within the plume as described below. The increase of the nitrogen oxides concentration in the upper troposphere leads to ozone production through the reaction of NO with peroxyde (HO_2), CH_3O_2, or RO_2 radicals from the OH oxydation as shown by the reaction $R1$.

$$NO + RO_2 \longrightarrow NO_2 + RO \tag{R1}$$

In the case of large NO_x injection by lightning, the NO_x content (~ 40 ppt in unpolluted atmosphere) becomes close (a few ppb, according to in-situ measurements, Dye et al. (2000); Huntrieser et al. (2002)) to the surrounding ozone (60 ± 24 ppb) (Jaéglé et al., 1998). The ozone evolution within the plume is described by the reactions R2-R6.

$$NO_2 + h\nu(\lambda < 400\text{nm}) \longrightarrow NO + O \tag{R2}$$

$$NO + O_3 \longrightarrow NO_2 + O_2 \tag{R3}$$

$$O + O_2 + M \longrightarrow O_3 + M \tag{R4}$$

$$O + NO_2 \longrightarrow NO + O_2 \tag{R5}$$

$$O + O_3 \longrightarrow 2O_2 \tag{R6}$$

From these equations we can define an O_x family ($O_x \equiv O + O_3 + NO_2$) where the only net loss of O_x is by reactions between atomic oxygen and NO_2 or O_3. The rate of change of each chemical family are given by the equations 5, 6 and 7 (Cariolle et al., 2009).

$$\frac{d([O] + [O_3])}{dt} = +k_2 \cdot [NO_2] - k_3 \cdot [NO] \cdot [O_3] - k_5 \cdot [O] \cdot [NO_2] - 2 \cdot k_6 \cdot [O_3] \cdot [O] \tag{5}$$

$$\frac{d([O] + [O_3] + [NO_2])}{dt} = -2 \cdot k_5 \cdot [O] \cdot [NO_2] - 2 \cdot k_6 \cdot [O_3] \cdot [O] \tag{6}$$

$$\frac{d([NO] + [NO_2])}{dt} = 0 \tag{7}$$

Where k_i correspond to the rate constants for the R_i reactions.

Thus two processes occur to O_3 in the plume at daytime. On short timescales O_x is conserved. Lightning emissions of NO in the plume are converted into NO_2 but as NO_2 is in O_x family, there is net conservation of O_x. However, on long timescales O_x can be destroyed through the reaction of O with NO_2 and O_3. Both of these processes need to be considered.

The first regime (regime I) occurs at low concentrations of NO_x (relative to O_3). Under these conditions the reaction R5 is slow. There is the rapid equilibrium between NO, NO_2 and O_3 (reactions R2, R3 and R4). As a consequence, O_3 is converted into NO_2 and can be restored later after dilution of the plume depending on the balance between NO and NO_2 at large scale (Cariolle et al., 2009). Overall O_x is conserved. In this regime NO emitted reacts with the available O_3 until the NO to NO_2 ratio in the plume reaches that in the background. Thus, the impact on the O_3 background concentration is to reduce it by the number of molecules of NO emitted multiplied by the background NO_2 to NO_x ratio. The effect of the first regime on the ozone burden is expressed by the equation 8.

$$\frac{\partial \overline{r_{O_3}}}{\partial t} + < F_{O_3} > = -\frac{1}{\tau} \cdot \overline{r_{LNO_x}} \cdot \alpha_{NO_x} \cdot (\frac{\overline{NO_2}}{\overline{NO_x}} - E) \cdot \delta + L_{ss} \tag{8}$$

Where, $\overline{r_{O_3}}$, is the mixing ratio of O_3 (in ppb) in the model grid, E is the $\frac{NO_2}{NO_x}$ ratio in the initial emissions, δ is equal to 1 during the day and 0 at nighttime, L_{ss} are the sources and sinks of ozone such as photochemical production, transport from the stratosphere, surface deposition, photolysis reactions, and photochemical destruction.

The second regime (regime II) occurs at high concentrations of NO_x (relative to O_3). Under these conditions the rate of R5 is large. The non-linear chemical interactions between NO_x and O_3 occur with different rates than in the background atmosphere. To account for this, Cariolle et al. (2009) introduced an effective reaction rate constant (K_{eff}), which is related to the production or the destruction of the odd oxygen (O_x) within the plume. K_{eff} is expressed by the equation 9.

$$K_{eff} = \frac{\int_{t_0}^{T_l} (\int_{V_p} K \cdot r_{NO_x}^P \cdot r_{O_3}^P \cdot \mathrm{d}V_p) \cdot \mathrm{d}t}{\overline{r_{O_3}} \cdot \int_{t_0}^{t_l} (\int_{V_p} r_{NO_x}^P) \cdot \mathrm{d}V_p) \cdot \mathrm{d}t} \tag{9}$$

Where $r_{NO_x}^P$ and $r_{O_3}^P$ are the mixing ratios of nitrogen oxides and ozone within the plume, $\overline{r_{O_3}}$ is the background ozone mixing ratio averaged in the model grid and K is the rate of NO_x-O_3 reaction within the plume.

The analysis of the chemical reactions related to the two regimes shows that $[O_3] \gg [O]$ and $k_5 \cdot [NO_2]$ is more efficient than $k_6 \cdot [O_3]$ as a sink for O_x (Cariolle et al., 2009). Thus, the equation 6 is simplified to give the equation 10.

$$\frac{d([O_3] + [NO_2])}{dt} = -2 \cdot k_5 \cdot [O] \cdot [NO_2] \tag{10}$$

Consequently, K_{eff} can be simplified to equation 11.

$$K_{eff} = \frac{2 \cdot (\int^T k_5 \cdot O \cdot NO_2 \cdot \mathrm{dt})}{(NO_x \cdot \int^T O_x \cdot \mathrm{dt})} \tag{11}$$

The calculation of K_{eff} is detailed in section 3.2.4. Considering the two regimes related to the sub-grid plume chemistry, the ozone burden is described by the equation 12 at daytime and nighttime. Note that at nighttime there is no direct impact due to the ozone plume chemistry on its burden as $\delta = 0$. Only indirect effects are expected from NO_y chemistry.

$$\frac{\partial \overline{r_{O_3}}}{\partial t} + < F_{O_3} > = -\frac{1}{\tau} \cdot \overline{r_{LNO_x}} \cdot \alpha_{NO_x} \cdot (\frac{\overline{NO_2}}{\overline{NO_x}} - E) \cdot \delta - K_{eff} \cdot \overline{r_{LNO_x}} \cdot \rho \cdot \alpha_{NO_x} \cdot \overline{r_{O_3}} \cdot \delta + L_{ss} \tag{12}$$

In addition, we consider the conversion of NO_x into HNO_3 within the plume. This conversion takes place in two different ways depending on the day or night atmospheric conditions. During the day, NO_2 reacts primarily with OH to give HNO_3 directly and it is characterized by the coefficient β_1. While at nighttime the conversion of NO_x to HNO_3 occurs mainly through the N_2O_5 formation followed by a heterogeneous hydrolysis reaction, which corresponds to β_2. In other words, the β coefficients are the molar fractions of NO_x converted to HNO_3 within the plume. These two fractions are unitless.

In summary, the equation system solved at large scale by the CTM for lightning NO_x source is detailed by the equations 13, 14 and 15.

$$\frac{\partial \overline{r_{NO_x}}}{\partial t} + < F_{NO_x} > = +\frac{1}{\tau} \cdot \overline{r_{LNO_x}} \cdot (1 - \beta_1 \cdot \delta - \beta_2 \cdot (1 - \delta)) \cdot \alpha_{NO_x} + L_{ss} \tag{13}$$

$$\frac{\partial \overline{r_{HNO_3}}}{\partial t} + < F_{HNO_3} > = +\frac{1}{\tau} \cdot \overline{r_{LNO_x}} \cdot (\beta_1 \cdot \delta + \beta_2 \cdot (1 - \delta)) \cdot \alpha_{NO_x} + L_{ss} \tag{14}$$

$$\frac{\partial \overline{r_{O_3}}}{\partial t} + < F_{O_3} > = -(\frac{1}{\tau} \cdot (\frac{\overline{NO_2}}{\overline{NO_x}} - E) + K_{eff} \cdot \overline{r_{O_3}} \cdot \rho) \cdot \overline{r_{LNO_x}} \cdot \alpha_{NO_x} \cdot \delta + L_{ss} \tag{15}$$

Where, $\overline{r_{NO_x}}$, $\overline{r_{HNO_3}}$ and $\overline{r_{O_3}}$, correspond to the NO_x, HNO_3 and O_3 mixing ratios averaged over the grid cell of the model, respectively.

In this study, the tropospheric chemistry and especially the LNO_x plume chemistry is considered both at daytime and nighttime since all reactions are not initiated during the day. The chemical interactions during the night correspond mainly to the reactions of O_3 and O with NO and NO_2 as well as the NO_x deactivation and the chemistry of the nitrogen reservoir species (here HNO_3 and

N_2O_5) and the nitrate radical (NO_3). NO_3 is the main oxidant in night conditions and is produced from the slow oxidation of NO_2 by O_3 (reaction $R7$).

$$NO_2 + O_3 \longrightarrow NO_3 + O_2 \quad \text{(R7)}$$

The other dominant source of NO_3 is the destruction of N_2O_5 (reaction $R8$), but as N_2O_5 is formed from NO_3 (reaction $R9$), the two species act in a coupled manner.

$$N_2O_5 + M \longrightarrow NO_3 + NO_2 + M \quad \text{(R8)}$$

$$NO_3 + NO_2 + M \longrightarrow N_2O_5 + M \quad \text{(R9)}$$

As mentioned previously, N_2O_5 is a determining species for the tropospheric chemistry at nighttime allowing the HNO_3 formation by the heterogeneous reaction on the particle surface (aerosols and ice crystals). During the day, NO_3 rapidly undergoes photolysis to produce NO or NO_2. In addition, NO_3 reacts very quickly with NO which is more concentrated at daytime than at nighttime (reaction $R10$) but NO_3 is very low at daytime. However, this reaction can take place during the night especially for a plume characterized by high NO mixing ratios (like a plume from lightning emissions) which is transported both during the day and night.

$$NO_3 + NO \longrightarrow NO_2 + NO_2 \quad \text{(R10)}$$

Furthermore, the nitrate radical can potentially reacts with VOCs. The reaction of the unsaturated hydrocarbons such as, isoprene, butenes, and monoterpenes, with NO_3 leads to the HNO_3 formation (Monks, 2005) (reaction $R11$).

$$NO_3 + RH \longrightarrow HNO_3 + R \quad \text{(R11)}$$

Considering NO_3 reaction with alkenes, an additional mechanism is found initiating a complex chemistry allowing to form NO_2 or organic nitrates (Monks, 2005). Finally, NO_3 can initiate the VOCs oxidation via peroxy radical production (reaction $R12$). That way, it can involve as a chain propagator (reactions R13 to R17).

$$NO_3 + \text{Organic Compound} \longrightarrow R + \text{Products} \quad \text{(R12)}$$

$$R + O_2 + M \longrightarrow RO_2 + M \quad \text{(R13)}$$

$$RO_2 + NO_3 \longrightarrow RO + NO_2 + O_2 \quad \text{(R14)}$$

$$RO + O_2 \longrightarrow R^{'} R^{''} CO + HO_2 \quad \text{(R15)}$$

$$HO_2 + O_3 \longrightarrow OH + 2O_2 \quad \text{(R16)}$$

$$HO_2 + NO_3 \longrightarrow OH + NO + O_2 \quad \text{(R17)}$$

The reactions of HO_2 with ozone ($R16$) or NO_3 ($R17$) imply OH production. Also, the reaction of ozone with alkenes allowing formation of OH during the night (reaction $R18$) (Aumont, 2005).

$$\text{Alkene} + O_3 \longrightarrow v_1 OH + v_2 HO_2 + v_3 RO_2 \quad \text{(R18)}$$

The reaction $R18$ occurs when ozone concentrations remain sufficiently high in night conditions, in other words for polluted atmosphere.

In this context, we consider different values at daytime and nighttime for the plume lifetime, the effective reaction rate constant and for the fraction of NO_x conversion into HNO_3 within the plume. Distinguishing day and night chemistry is linked with the fluctuation of the critical r_l value (below which the sub-grid plume chemistry is negligible) depending on atmospheric conditions. Therefore, if r_l changes with sunlight, the plume lifetime changes also. Note that except the β_2 fraction, this night chemistry is not considered by the initial plume approach developed by Cariolle et al. (2009), which considers NO_x plumes from aircraft exhausts only at daytime.

Figure 1 summarizes all elements which define the plume approach and how it has been adapted and implemented into the model.

3.2 Parameter calculations for lightning NO_x emissions

In order to reproduce more accurately the lightning NO_x sub-grid chemistry, some points should be considered: (i) the latitude (NO_x emissions by lightning are higher in tropics than in mid-latitudes); (ii) the sunlight conditions (day and night) which impacts photochemistry and heterogeneous chemistry; (iii) the plume evolution with its own physical characteristics (the lifetime and the dispersion properties); and finally (iv) chemical interactions within the plume related to highly elevated NO_x concentrations relative to the background. In the following section, physical and chemical characteristics of the plume associated with lightning NO_x source have been defined.

3.2.1 Dynamical conditions

The horizontal diffusion coefficient (D_h) is a key parameter of the atmospheric dynamical conditions in determining the dispersion of the lightning NO_x plume. D_h is used as the dispersion constraint

for the simple plume dispersion simulations carried out in order to estimate the plume lifetime and the effective reaction rate constant. The diffusion coefficient was determined by two different ways. A first estimate of the horizontal diffusion was performed by running the 3-D mesoscale Meso-NH model. Then, the D_h coefficient was calculated using in-situ measurements in thunderstorm anvil.

The Meso-NH mesoscale model was used (see section 2.2) to investigate D_h. A simple convective cell forced by warm bubble and initialized by a radiosounding at the simulation start was run as an ideal case. Simulations were realized for a domain of 24 km in the two horizontal directions and the grid horizontal resolution is $\Delta x = \Delta y = 1$ km and $\Delta z = 500$ m. The convective cell is located at $43.29° N$ latitude and $0°$ longitude (Klemp and Wilhelmson, 1978). Simulations of 6 hours were performed allowing the complete development and the dissipation of the convective cell. D_h has been calculated within the anvil using the mixing length diagnostic variable, hereafter denoted L, as described by the equation 16 (Cuxart et al., 1999).

$$D_h = \frac{2}{3} \times \frac{L}{4} \times \exp(\frac{1}{2}) \tag{16}$$

At the mature stage of the cell, D_h was calculated as $100\ m^2 \cdot s^{-1}$ within the upper levels of the convective cell (i.e. in the anvil, defined empirically).

In addition to modeling estimate, we used in-situ measurements to calculate D_h. Turbulence measurements were performed by a B-757 commercial aircraft along a flight from the west of Kansas to the north of Missouri and corresponding to a trajectory of more than 500 km (Trier and Sharman, 2008). These in-situ measurements were accomplished from 0700 to 1000 UTC the 17 June, 2005, during the development of a mesoscale convective system (MCS). This MCS is associated with a turbulence event characterized by the measurement of the atmospheric eddy dissipation rate (ϵ) and the turbulence kinetic energy (TKE) above and within the cloud anvil. The higher values of ϵ ($\epsilon^{1/3} \sim 0,4\ m^{2/3} \cdot s^{-1}$) were recorded between 11.3 and 11.6 km altitude corresponding to the cloud anvil levels. In addition, for this MCS, the TKE was about $1\ m^2 \cdot s^{-2}$ at the locations of the highest ϵ values.

According to these observations, the turbulent diffusivity (equation 17) was estimated above the anvil of the MCS (http://www.ral.ucar.edu/projects/turb_char/) such as: $D_h > 0.1\ m^2 \cdot s^{-2}$. Then, D_h was calculated within the anvil such as: $D_h = 15\ m^2 \cdot s^{-1}$ using the same formulation (equation 17). This last estimate seems to be the most common value compared to the diffusion coefficient value of $20\ m^2 \cdot s^{-1}$ used by Cariolle et al. (2009), close to the tropopause level and the D_h value calculated for contrails ($15\ m^2 \cdot s^{-1}$) in the upper troposphere (Knollenberg, 1972).

$$D_h = \frac{(TKE)^2}{\epsilon} \tag{17}$$

The D_h estimate using Meso-NH model is high compared to the results from measurements and corresponds to the upper limit of the calculated diffusion coefficients and could be associated with the turbulence in the convective cloud. However, it is important to note that usually most numerical simulations are performed with 1-D turbulence models. What is interesting in the use of Meso-NH in this study is that the 3-D turbulence is solved. This simulation provides an additional estimate of D_h allowing comparison with the calculation from in-situ measurements. Moreover, studies on the diffusivity in cloud anvils are uncommon. It is necessary to conduct additional work in the future on that issue again constrained with new in-situ measurements of the atmospheric turbulence in the anvil.

It is important to note that the 3-D turbulence is not solved online in the GEOS-Chem model because of the fine scale characterizing this process but prescribed by the GEOS-5 met fields. Therefore, the global variability of D_h is not calculated by the CTM and it is beyond the scope of this study.

In order to cover all horizontal diffusivity estimates discussed in this section the range of values 0.1, 15 and 100 $m^2 \cdot s^{-1}$ was used. The horizontal coefficient is constant for all lightning NO_x plumes which are considered in the GEOS-Chem model. Hereafter, the results are detailed for the central value $D_h = 15\ m^2 \cdot s^{-1}$. Sensitivity tests depending on the uncertainty associated with the parameter estimate are performed and presented later in section 4.3.

3.2.2 The NO_x critical plume content (r_l)

The r_l critical value is the NO_x mixing ratio within the undiluted phase of the plume below which the non-linear chemistry can be neglected (section 3.1). It has been estimated using the 0-D DSMACC chemical box model (section 2.2). Initial conditions for simulations carried out with the DSMACC box model are from outputs of the GEOS-Chem model. Especially, initial atmospheric parameters and atmospheric background concentrations of species correspond to the average of the GEOS-Chem outputs (i) from 8 km to 11 km, (ii) for two latitude regions (tropics and mid-latitudes), and (iii) for the year 2006 (table 1). The altitude range refers to the detrainment region estimated by GEOS-Chem using the GEOS-5 met fields (section 2.1) both in the tropics and in the mid-latitudes. Note that this range could vary depending on the met fields and the convection parameterization. In addition, the LNO_x plume parameterization should have an impact outside of this altitude range mainly between 6 km and 12 km but in a lesser extent.

In order to focus on chemistry interactions only between chemical species of interest and removing the mixing influence and sunlight fluctuations, short simulations (i.e. one hour each) were run with the DSMACC model. The effects of the day or night conditions were carefully considered carrying out separate simulations at daytime and nighttime. Simulations were run for a large range of

initial NO mixing ratios from 0.01 ppb to 1 ppm. The r_l value is defined from the NO value for which the $\frac{\partial O_x}{dt}$ trend is perturbed. In other words, r_l is associated to the second derivative of O_x, i.e. the curve optimums on figure 2. The r_l threshold was defined as to be 0.1 and 0.25 ppb during the day and night for mid-latitudes and 0.1 and 0.75 ppb during the day and night in the tropics (figure 2).

Note that the mid-latitudes and the tropics were separated because of the large differences in $LNOx$ emissions between the two regions in terms of the number of flashes in a particular convective cell which is higher in the tropics according to the LIS/OTD climatologies (Christian et al., 2003). This last point is important for the plume lifetime estimate detailed in the following section.

3.2.3 The plume lifetime τ

The plume lifetime (τ) depends directly on (i) the initial NO pulse from lightning emissions, (ii) the r_l critical value, and (iii) the diffusion properties of the atmosphere. The plume lifetime also depends on the initial size of the plume. Here we use a width of 500 m to refer to an ensemble of spikes at the cloud scale (i.e. each plume is defined from several electrical discharges at a convective cell scale). τ is crucial for the physical description of the NO_x plumes and it has been computed in carrying out dispersion simulations of a simple plume assumed to be cylindrical. In this model, the standard atmospheric conditions are represented by temperature, pressure and species concentrations of the background atmosphere, which are similar to the initial conditions used for the DSMACC simulations. As a reminder, initial conditions are from GEOS-Chem outputs averaged (i) from 8 km to 11 km, (ii) for two latitude regions (tropics and mid-latitudes), and (iii) for the year 2006 (table 1). Simulations are initialized by a NO pulse from lightning emissions (hereafter denoted NO_i) and the plume dispersion depends on the D_h value estimated in section $3.2.1$.

The initial tracer concentrations NO_i related to lightning NO emissions at the scale of a convective cell (gathering several flashes together) in mid-latitudes were defined according to previous aircraft measurement campaigns. Especially, the STERAO campaign recorded NO spikes of magnitude from 1-10 ppb related to lightning activity in thunderstorms occurring 9-10 July 1996 over northern Colorado (Dye et al., 2000; Stith et al., 1999). Lange et al. (2001) measured NO spikes of 3.5 ppb during the STREAM campaign associated with a matured storm over Ontario. Several peaks of NO mixing ratios from 0.7-6 ppb were also observed during EULINOX (Huntrieser et al., 2002) over Germany in July 1998. The LINOX aircraft campaign recorded NO spikes from 0.75-1.25 ppb (Huntrieser et al., 1998) related to thunderstorm over Europe, the 30 July 1996. From these studies, the NO concentration associated with the electrical activity in thunderstorms occurring over the mid-latitudes was determined as $NO_i^{mean,Midlats}$ = 3.4 ppb ($NO_i^{min,Midlats}$ = 0.7 ppb and $NO_i^{max,Midlats}$ = 10 ppb). Because there are much fewer LNO_x measurements in the tropics and in order to be consistent with the LNO_x emissions defined in the GEOS-Chem model,

the ratio $R_{LNO_x} = \frac{LNO_x^{Midlatitudes}}{LNO_x^{Tropics}}$ was defined as in the CTM. During the year 2006, the relative mid-latitudes and tropics LNO_x contribution was about $R_{LNO_x} = 0.33$. This result is in agreement with higher LNO_x emissions in these regions rather than in the mid-latitudes. The value of NO mixing ratio injected by lightning in the tropics was estimated as $NO_i^{mean,Tropics}$ = 10.2 ppb ($NO_i^{min,Tropics}$ = 2.8 ppb and $NO_i^{max,Tropics}$ = 29.7 ppb).

Once NO_i estimate was completed, the calculation of the plume lifetime was achieved using the detailed formulation given in section 3.1.1. The results for τ are summarized in table 2. Hereafter, the results are detailed for NO_i^{mean} in section 4 and sensitivity tests are carried out using all NO_i values for the mid-latitudes and the tropics (section 5). Model calculations for NO_i^{mean} and $D_h = 15\ m^2 \cdot s^{-1}$ provide a minimum plume lifetime of 3 (6) hours for the mid-latitudes and maximum plume lifetime of 9 (21.3) hours for the tropics at daytime (nighttime).

3.2.4 The effective reaction rate constant (K_{eff})

The non-linear chemistry within the plume has been considered in calculating the effective reaction rate constant (K_{eff}), which is used to compute the formation of the secondary species (O_x and HNO_3) within the plume. That corresponds to the evolution of odd oxygen depending on the O and O_3 reactions with NO_2 and NO, and also on the NO_x activation (day) or deactivation (night) with the HNO_3, N_2O_5 and PAN chemistry. Note that in the case of lightning emissions other species like VOCs, HO_x and H_2O may be uplifted in the convective region. However, we assumed that the OPE is mainly controlled by NO_x in the upper troposphere as previously showed by Sauvage et al. (2007b). Therefore, K_{eff} calculation is here mainly dependent on NO_x content. Future studies should try to investigate this issue for lightning emissions mixed with strong surface emissions in order to sharpen our parameterization.

K_{eff} is calculated according to the equation 11 of the section 3.1.2 using the same simple plume dispersion simulations than those carried out to define the plume lifetime (section 3.2.3).

Results for K_{eff} are summarized in table 3. Model calculations using NO_i^{mean} and $D_h = 15\ m^2 \cdot s^{-1}$ give a K_{eff} value of $5.49 \cdot 10^{-19}\ molecules^{-1} \cdot s^{-1} \cdot cm^3$ ($4.55 \cdot 10^{-19}\ molecules^{-1} \cdot s^{-1} \cdot cm^3$) in the mid-latitudes and $3.64 \cdot 10^{-19}\ molecules^{-1} \cdot s^{-1} \cdot cm^3$ ($2.98 \cdot 10^{-19}\ molecules^{-1} \cdot s^{-1} \cdot cm^3$) in the tropics, at daytime (at nighttime).

Our K_{eff} estimates are smaller than those calculated by Cariolle et al. (2009) for the plume chemistry related to aircraft exhausts. In this previous work, K_{eff} varies from 1.0 to $4.2 \cdot 10^{-18}\ molecules^{-1} \cdot s^{-1} \cdot cm^3$ with a mean value close to $3 \cdot 10^{-18}\ molecules^{-1} \cdot s^{-1} \cdot cm^3$ depending on the NO_x load-

ing. The very low value for K_{eff} point out that the plume parameterization implies a delay of the production of ozone at the large scale rather than its destruction within the plume.

3.2.5 The fractions of NO_x conversion to HNO_3 (β_1 and β_2)

The fractions β_1 and β_2 represent the NO_x conversion into HNO_3 within the plume at daytime and nighttime respectively. They were computed using the DSMACC chemical box model.

The β_1 coefficient was calculated for day conditions depending mainly on the OH concentration. The conversion of NO_x into HNO_3 at nighttime (β_2 coefficient) is related to the heterogeneous reaction of N_2O_5 and so depends on particles (aerosols and ice crystals) concentration and their lifetime. This is directly linked with the surface density and the radius of particles in the anvil region of thunderstorms, which is highly uncertain. We defined these values using in situ measurements. The surface area (S_T) and the radius (R) for aerosols are defined such as: $S_T = 0.28\ m^{-1}$ and $R = 1\ \mu m^{-1}$ (Huntrieser et al., 2002) and for ice, $S_T = 0.03\ m^{-1}$ and $R = 30\ \mu m^{-1}$ (Knollenberg et al., 1993). In addition, the reaction probabilities of NO_x on aerosols and ice crystals $\gamma_{N_2O_5}^{aerosols} = 0.02$ (Evans and Jacob, 2005) and $\gamma_{N_2O_5}^{ice} = 0.03$ (Sander et al., 2006), respectively, were used for our box model simulations. These values correspond to the probability that a N_2O_5 molecule impacting an aerosol or an ice crystal surface was subjected to react. The results for β_1 and β_2 coefficients are summarized in table 4.

The estimate of β_1 fraction does not show significant variation neither between latitudes regions nor depending on NO_i. The minimum β_1 value is $1.34 \cdot 10^{-4}$ for the tropical regions and NO_i^{min}, and the maximum β_1 value is $1.88 \cdot 10^{-4}$ for the mid-latitudes and NO_i^{max}. The study of production and destruction rates for day conditions taking into account all reactions pathways (not shown here) demonstrates that production of HNO_3 during the day is mainly determined by reaction of NO_3 with formaldehyde ($HCHO$) and acetaldehyde (CH_3CHO). Surprisingly, the HNO_3 formation via the $NO_2 + OH$ reaction seems to be less efficient. This result could be explained by the low initial concentrations of OH used for the DSMACC simulations and it is in agreement with the small β_1 values. Then, the averaged β_2 coefficient is higher by a factor 10 compared to β_1 with a minimum value of $0.24 \cdot 10^{-3}$ in the tropics for NO_i^{max} and a maximum estimate of $14.4 \cdot 10^{-3}$ in the mid-latitudes for NO_i^{min}. The analysis of the production and the destruction rates for night conditions taking into account all reactions pathway shows that the predominant reaction in the HNO_3 evolution is $N_2O_5 + H_2O$ (or the heterogeneous reaction on the aerosols and ice crystals surface).

4 Results: CTM simulations

In this section, the effects of the lightning NO_x plume parameterization, i.e. the influence of the sub-grid processes related to lightning emissions, on the NO_x and O_3 tropospheric distributions at large scale are evaluated. Then, the parameterization sensitivity to initial NO mixing ratio injected by lightning (NO_i), D_h, β_1 and β_2 coefficients is analyzed to quantify the variability of the results regarding the plume-in-grid parameter calculations.

4.1 Implementation of the LNO_x plume parameterization

The implementation of the lightning NO_x plume parameterization into the GEOS-Chem model requires specifying the system of continuity equations related to the plume chemistry solved at large scale by the model (section 3.1.2, equations 13, 14 and 15). Lightning NO_x emissions calculated in each grid box (in $molecules \cdot cm^{-2} \cdot s^{-1}$) by the model are directly used to compute the injection rate I (s^{-1}) of NO at each chemical time step of the simulation. Then, we consider that $\alpha_{NO_x} = 1$ in order to represent the mixing ratio of the undiluted fraction of NO_x by the tracer (r_{LNO_x}). Furthermore, lightning produce negligible quantities of NO_2 relative to NO and therefore E is 0 in the equation 15. Finally, the ratio $\frac{\overline{NO_2}}{\overline{NO_x}}$ is the relative balance between NO and NO_2 in the diluted phase at large scale reproduced by the model.

4.2 Impact of LNO_x emissions on the NO_x and O_3 distributions

We perform a spin-up of six months (from July 2005 to January 2006) in order to obtain a steady state in the model after activation of the plume parameterization. Then, simulations were run for the entire year 2006. The transport and the convection time steps are 15 minutes and the emissions and the chemical time steps are 30 minutes.

In the following, standard simulation refers to simulation with standard lightning NO_x emissions i.e. instantaneously diluted in a grid cell, while modified simulation refers to simulation considering the plume parameterization and then sub-grid chemistry. Note that the modified simulation was run using mean values for the initial NO mixing ratio ($NO_i^{mean,Midlats} = 3.4\ ppb$ et $NO_i^{mean,Tropics} = 10.2\ ppb$) and $D_h = 15\ m^2 \cdot s^{-1}$. The Base Case (BC) experiment corresponds to the standard simulation minus the standard simulation without lightning NO_x emissions. The $P1$ experiment corresponds to the modified simulation minus the standard simulation without lightning NO_x emissions. The $P2$ experiment is the same as the $P1$ experiment but without considering the nitrification mechanism in the modified simulation (i.e. $\beta_1 = \beta_2 = 0$). In addition, sensitivity tests were performed for $P1$ defined by the modified simulation using the minimum and the maximum values for D_h, NO_i, β_1 and β_2 coefficients. All experiments are summarized in table 5.

Lightning emissions rates and the associated LNO_x tracer distributions are first discussed, then the effects of the implementation of the plume parameterization ($P1$) compared to the experiment without the plume-in-grid development (BC case) is presented.

4.2.1 Lightning emissions and LNO_x tracer distributions

Figure 3 displays the geographical distributions of the 9 km lightning NO_x emissions (a), the related LNO_x tracer distributions (b) and the LNO_x tracer zonal averaged (c) in January (top panels) and in July (bottom panels) reproduced by the CTM from the $P1$ experiment. These results are shown for an approximate detrainment level (9 km altitude) where the detrainment of LNO_x is the largest. In January, the highest emissions of NO_x from lightning ($4-6\cdot10^9\ molecules\cdot cm^{-2}\cdot s^{-1}$) are located in the southern hemisphere around the tropics over West Australia and Central-South Africa. Also, the model gives low LNO_x emissions ($<3\cdot10^9\ molecules\cdot cm^{-2}\cdot s^{-1}$) over South America and North America especially over the Gulf of Mexico. In July, the highest LNO_x emissions ($4-6\cdot10^9\ molecules\cdot cm^{-2}\cdot s^{-1}$) are calculated in the northern hemisphere over North America, North of India, Central Africa and Sahel. In addition, LNO_x emissions are modeled over Europe and over East Asia but to a lesser extent ($<2\cdot10^9\ molecules\cdot cm^{-2}\cdot s^{-1}$).

The lightning NO_x tracer introduced into the model represents the lightning NO_x emissions affected by the transport and the exponential decay depending on the plume lifetime. Figure 3 shows that the tracer distribution is consistent with the lightning NO_x emissions. However, it is important to note that the plume lifetime is a key factor in the evolution of the LNO_x tracer mixing ratio. A long plume lifetime (several hours to several days) allows the intercontinental transport of LNO_x plumes. The representation of the sub-grid chemistry and the transport of the non-linear chemistry effects related to the plume consideration becomes important for the chemistry of the regions located far downwind from source regions. The plume lifetime depends on the latitude because of the different background chemical concentrations and the different amount of NO_x emitted from lightning in the tropics and in the mid-latitudes. In addition, as mentioned before, we consider the influence of day and night conditions on the plume lifetime estimate. According to its preliminary calculation (section 3.2.3), the plume lifetime is longer in the tropics (9 and 21.3 hours for day and night conditions, respectively) than in the mid-latitudes (3 and 6 hours, for day and night conditions, respectively). So, the LNO_x tracer is characterized by a shorter lifetime as a plume over North America than over Central Africa and around the Sahel while the model simulated fewer emissions over these regions especially in summer. In boreal winter, the mixing ratio of the lightning NO_x tracer calculated by the model is about 0.21 ppb over Central and South Africa, 0.18 ppb over West Australia and 0.11 ppb over South America. In summer, the tracer mixing ratio is simulated as 0.21 ppb, 0.32 ppb and 0.16 ppb over Central Africa, North India and North America, respectively.

The lightning NO_x tracer is produced at altitudes where lightning NO_x are calculated and detrained (in the upper troposphere between ~ 500 and 300 hPa) as shown in panels (c) in figure 3.

4.2.2 Impact of lightning on NO_x and O_3 distributions with the plume parameterization

The difference between $P1$ and BC experiments $(P3)$ was calculated in order to quantify the changes on NO_x and O_3 mixing ratios at large scale implied by the implementation of the plume-in-grid parameterization into GEOS-Chem. Figures 4 and 5 display the geographical distributions of the NO_x, HNO_3, PAN and O_3 absolute changes (in ppb) in January and in July, respectively. The 9 km altitude level was chosen because of the most significant variations at this altitude compared to the rest of the troposphere.

In boreal winter, LNO_x plume chemistry leads to a maximum decrease at large scale over regions of emissions of 120 ppt for NO_x and a decrease of 68 ppt for HNO_3 and 16 ppt for PAN over Central and South Africa. These variations are associated with a maximum O_3 decrease of 2.8 ppb over regions of emissions. A similar NO_x, HNO_3, PAN and O_3 reduction is obtained in other areas of high LNO_x emissions (i.e. over West Australia and South America). Downwind of LNO_x emissions, the opposite effect is observed for NO_x and HNO_3 species with maximum increase of 40 ppt for NO_x and 13.5 ppt for HNO_3 observed over South Atlantic and Indian Ocean. Generally, PAN still decreases over oceans but in a lesser extent compared to regions of LNO_x emissions, with a maximum reduction of 9 ppt. O_3 response is a maximum increase of 1.13 ppb around area where the transport is effective and especially over the oceans. In summer, maximum decreases of 140 ppt for NO_x and 60 ppt for HNO_3 and 24 ppt for PAN are calculated by the CTM leading to a maximum O_3 decrease of 2.4 ppb over Central Africa (reduction also observed over North America and North India). Downwind of lightning emissions, increase of NO_x and HNO_3 is observed with a maximum value of 30 ppt and 38 ppt, respectively. PAN reservoir species also still decreases slightly downwind with 2 ppt changes. Finally, that leads to maximum O_3 increase of 0.7 ppb.

Note that the production of PAN is limited by the supply of NO_x or non-methane volatile organic compounds (NMVOCs). Above continental lightning sources regions, NMVOCs are uplifted by deep convection but with lower NO_x due to the activation of the plume parameterization. That implies a less efficient PAN production in these regions. Downwind of lightning sources regions (oceanic regions), NO_x increases because of the LNO_x transport in the plume form but there is less NMVOCs available to produce PAN. Therefore, both in regions of LNO_x emissions and downwind, the PAN production is limited leading to overall lower PAN mixing ratios at large scale in P1 experiment. However, this may be nuanced by considering the PAN chemistry in future studies using similar LNO_x plume parameterization by introducing the PAN and CH3C(O)OO continuity equations and a new term to consider the fraction of NO_x converted to PAN within the plume. This

should allow the PAN production during the plume transport, which is inhibited in the current version.

In order to provide a full overview of the effects of the plume parameterization, the relative difference between the $P1$ and BC experiments (i.e. $P3/BC$) was calculated integrated throughout the troposphere. Figures 6 and 7 show zonal averaged of NO_x (upper panels) and O_3 (bottom panels) relative changes (in %) integrated throughout the troposphere for regions of interest for January and July, respectively. During boreal winter, the highest NO_x (O_3) decreases of 10 % (5 %) in West Australia, then 20 % (6 %) in Central Africa are calculated. These negative variations are mainly calculated between 400 hPa and the tropopause level for NO_x and ozone. South America is characterized by a decrease of 20 % of the nitrogen oxides and 1 % of ozone. Over this region, variations are significant in the entire troposphere for both species. In contrast to the continent decrease, NO_x increase is observed over the major part of South Atlantic and Indian Ocean with 14 % and 20 % maximum, respectively. The O_3 response in an increase of 1 % near the tropopause and it becomes higher close to the surface of about 4 %. In summer, there is a NO_x (O_3) decrease of 25 % (8 %) over Central Africa, 20 % (2 %) over North India, and 5 % (0.5 %) over North America. Also, South Atlantic and Indian Ocean (located downwind of lightning NO_x emissions) are characterized by a maximum increase of 18 % for NO_x and 2 % for O_3.

As a result, the sub-grid chemistry associated to the LNO_x emissions implies (i) a decrease of the nitrogen oxides and ozone mixing ratios at large scale over regions characterized by intense lightning emissions and (ii) an increase of these species downwind of emissions. Especially the plume parameterization related to the lightning NO_x leads to:

1. Significant effects on NO_x mixing ratio (± 20 %): these effects on nitrogen oxides are important because NO_x is the first criterion which is constrained in a CTM in order to determine the global LNO_x production ($6\ TgN \cdot yr^{-1}$ in the GEOS-Chem model);

2. Lower effects on O_3 mixing ratio (± 5 %): these limited impacts on ozone could be explained by compensatory effect of the NO_y species (mainly conversion of NO_x into HNO_3 within the plume).

The effects of the plume parameterization are simulated over the entire troposphere mainly for ozone. Indeed, the spreading of effects on ozone to the lower free troposphere is related to the subsidence areas of the Walker circulation. These regions are characterized by the accumulation and creation of ozone for low altitude levels. Nevertheless, the maximum NO_x and O_3 variations are calculated for altitude levels associated with a mean detrainment level. The more realistic representation of the sub-grid processes ($P1$ experiment) related to the LNO_x plume is in contrast with the simplified

instantaneous dilution in the grid cell of the lightning NO_x emissions (BC experiment).

The plume approach allows the conversion of NO_x into HNO_3 during the plume lifetime. In addition, the high NO_x concentration within the plume (much higher than the background content) leads to the O_3 titration and more generally to the O_x destruction within the plume. The most important impact of the plume parameterization is the transport of the LNO_x emissions as a plume and the transport of the associated non-linear chemistry effects leading to a delay of the O_3 production at large scale. In other words, O_3 is less produced over the regions with intense lightning NO_x emissions than downwind of LNO_x emissions by photochemical reactions from NO_x.

4.3 Plume sensitivity to the estimated uncertainties of parameter calculations

4.3.1 The Atmospheric dynamical conditions and the initial NO mixing ratio injected by lightning

The impact of (i) the diffusion properties of the atmosphere (D_h) and (ii) the initial NO mixing ratio injected by lightning (NO_i) are analyzed. D_h and NO_i are the two key parameters in the determination of the physical and chemical characteristics of the plume. The modified simulation characterizing the $P1$ experiment was run for the ranges of the horizontal diffusion coefficients and the initial NO mixing ratio injected by lightning. It is important to note that for these sensitivity tests, β_1 and β_2 coefficients remain constant using their mean values. τ and K_{eff} values related to these simulations are those previously calculated (section 3) and summarized in tables 2 and 3. Figure 8 displays τ (upper panels) and K_{eff} (bottom panels) variations depending on D_h and NO_i. As expected, the strongest the horizontal diffusion is the most efficient the dispersion of the plume is. In both, the mid-latitudes and the tropics, τ decreases when D_h becomes larger. In addition, τ increases with the initial NO mixing ratio injected by lightning. In contrary, K_{eff} increases with D_h coefficient in the two regions of the globe.

The sensitivity of the NO_x and O_3 mixing ratios around the mean value for regions and seasons depending on the known uncertainties associated with parameter calculations have been quantified. Figure 9 shows the ranges of sensitivity of NO_x and O_3 (ΔNO_x and ΔO_3, respectively) at 9 km altitude reproduced by GEOS-Chem depending on D_h and on the initial NO mixing ratio (NO_i). Note that for the sake of readability, the scale of NO_x and O_3 changes differs by region. Results are also summarized in table 6.

We chose representative continental areas such as Florida and Congo, which correspond to regions characterized by intense electrical activity for the mid-latitudes and the tropics, respectively. North and South Atlantic were selected to represent regions downwind of NO_x emissions, for the

mid-latitudes and the tropics variations, respectively. The highest NO_x and O_3 ranges are obtained for continental tropical regions with ΔNO_x $[-33.1; +29.7]$ ppt and ΔO_3 $[-1.56; +2.16]$ ppb, in January, and ΔNO_x $[-14.3; +21]$ ppt and ΔO_3 $[-1.18; +1.93]$ ppb, in July. The largest range associated with the tropical continents could be explained by the largest difference on parameter values defining the plume in this region (especially NO_i). The smallest changes are observed over continental mid-latitude regions for winter with ΔNO_x $[-1.7; +1.8]$ ppt and ΔO_3 $[-0.16; +0.72]$ ppb and over oceanic tropical regions in summer such as ΔNO_x $[-11.5; +2.6]$ ppt and ΔO_3 $[-0.14; +0.92]$ ppb. As a result, the sensitivity of NO_x and O_3 species to the parameter uncertainties is a few ppt for NO_x and less than 2 ppb for O_3.

4.3.2 Coefficients related to the nitrification mechanism (β_1 and β_2)

In order to estimate the sensitivity of the NO_x and O_3 mixing ratios related to the uncertainties on β_1 and β_2 fractions (table 7), the difference between $P1$ experiment using β_1 and β_2 mean values and $P1$ experiment using minimum and maximum β_1 and β_2 coefficients has been calculated. This implies that τ and K_{eff} are constant.

In January, the highest sensitivity on NO_x mixing ratio is ΔNO_x $[-2.3; +0.9]\cdot 10^{-2}$ ppt over the continental tropical regions and ΔO_3 $[-10; +11]\cdot 10^{-4}$ ppb over the tropical ocean on O_3, while the mid-latitudes oceanic areas show minimum ranges on NO_x and O_3 with $\Delta NO_x \pm 2.3 \cdot 10^{-2}$ ppt associated with ΔO_3 $[-9; +4]\cdot 10^{-4}$ ppb. In July, the maximum ranges are calculated over oceans in the mid-latitudes for NO_x such as ΔNO_x $[-21.1; +6.6]\cdot 10^{-2}$ ppt and in the tropics for O_3 with ΔO_3 $[-30; -2]\cdot 10^{-4}$ ppb. Finally, the smallest changes, ΔNO_x $[-0.9; -0.4]\cdot 10^{-2}$ ppt and ΔO_3 $[-24; -6]\cdot 10^{-4}$ ppb, are simulated for the tropical ocean and the mid-latitudes continent, respectively.

In addition, the impact of the nitrification mechanism was assessed comparing the $P1$ experiment using mean β_1 and β_2 values and $P2$ experiment for which $\beta_1 = \beta_2 = 0$. As a result, taking into account NO_x conversion into HNO_3 using the mean β fractions calculated in this study does not imply strong changes in NO_x and O_3 distributions ($\Delta NO_x < 10^{-4}$ ppb and $\Delta O_3 < 10^{-2}$ ppb).

In the case of significant values of β fractions, the rate of the nitrification mechanism should imply a delay of the O_3 formation from the NO_x in the plume because of the NO_x storage in HNO_3. On the other hand, HNO_3 is considered as a one of the main sink for NO_x species undergoing wet deposition and seemingly limiting their affect on global ozone.

The sensitivity tests point out the limited effect of the NO_x conversion to HNO_3 within the plume using our β_1 and β_2 calculations. The sensitivity on NO_x and O_3 mixing ratios related to β

coefficients is about a few ppt. Indeed, our β_1 and β_2 estimates are smaller than those calculated by Cariolle et al., 2009 ($\beta_1 = 0.06$ and $\beta_2 = 0.2$), which showed a large impact of this mechanism in the case of aircraft NO_x emissions. In the present study, we can easily suppose that the increase of the β_1 and β_2 coefficients should be in agreement with the work of Cooper et al. (2014) in reducing the underestimate of the HNO_3 production induced by NO_x emissions from lightning. Further estimates of β should be realized using future observations in cloud anvil of primary species, aerosols and particules needed for NO_x conversion at daytime and nighttime to improve the determination of these parameters. The β_1 coefficient is particularly dependent on the HO_x radicals, which could vary significantly within the cloud anvil in part because of the transport of peroxides from the lower troposphere by convective uplift (Wennberg et al., 1998). Then, the determination of β_2, corresponding to the NO_x conversion fraction into HNO_3 via N_2O_5 formation during nighttime is considerably dependent on (i) the estimate of aerosols and the ice crystal concentration and their lifetime within the cloud anvil which is highly uncertain according to measurement campaigns and (ii) on the reaction probability on aerosols $\gamma_{N_2O_5}^{aerosol}$ and ice crystals $\gamma_{N_2O_5}^{ice}$ from laboratory studies extrapolations.

According to results presented in this section, the sensitivity tests show the predominance of the initial NO mixing ratio injected by lightning (NO_i) and the diffusion properties of the atmosphere (D_h) in the variability of the NO_x and O_3 mixing ratios around the mean value in response to the plume-in-grid parameterization in the CTM. In winter, the NO_x and O_3 sensitivity is the highest for continental regions in the tropics and the smallest sensitivity is calculated for the mid-latitudes. In summer, the most important sensitivity of NO_x and O_3 is simulated in the tropics over regions characterized by intense LNO_x emissions while the least significant sensitivity is obtained still in the tropics but downwind of emissions (mainly over oceans).

5 Conclusions

For the first time, a more realistic lightning NO_x chemistry is implemented as a plume parameterization into a global chemical transport model. The key parameters characterizing the lightning-related plume were estimated depending on two main criteria, i.e. the NO mixing ratio injected by lightning (NO_i) and the atmospheric diffusion coefficient (D_h).

According to the NO_i and D_h ranges, the plume lifetime (τ) and the effective reaction rate constant (K_{eff}) for NO_x-O_3 chemical interactions were estimated as follow:

- $\tau = [0.01; 68.5]$ hours;
- $K_{eff} = [0.77; 23] \cdot 10^{-19}\ molecules^{-1} \cdot s^{-1} \cdot cm^3$.

Also, for the conditions defined by NO_i^{mean} and $D_h = 15\ m^2 \cdot s^{-1}$:

- τ is 3 (6) hours in the mid-latitudes and 9 (21.3) hours in the tropics at daytime (nighttime);
- K_{eff} is $5.49 \cdot 10^{-19}\ molecules^{-1} \cdot s^{-1} \cdot cm^3$ ($4.55 \cdot 10^{-19}\ molecules^{-1} \cdot s^{-1} \cdot cm^3$) in mid-latitudes and $3.64 \cdot 10^{-19}\ molecules^{-1} \cdot s^{-1} \cdot cm^3$ ($2.98 \cdot 10^{-19}\ molecules^{-1} \cdot s^{-1} \cdot cm^3$) in the tropics at daytime (nighttime).

Finally, the fractions of NO_x conversion into HNO_3 within the plume are $\beta_1 = [1.34; 1.88] \cdot 10^{-4}$, and $\beta_2 = [0.24; 14.4] \cdot 10^{-3}$ for day and night conditions respectively.

GEOS-Chem simulations performed using mean value for NO_i and $D_h = 15\ m^2 \cdot s^{-1}$ reveal nitrogen species and ozone changes compared to the instantaneous dilution. A decrease of NO_x and O_3 mixing ratios at large scale over the regions of strong LNO_x emissions is observed mainly in the northern hemisphere in summer and in the southern hemisphere in winter. In the troposphere, maximum decrease of 20 % (6 %) in January and 25 % (8 %) in July for NO_x (O_3), are found over Central Africa. In contrast, an increase of NO_x (O_3) downwind of emissions is simulated of 20 % (4 %) in January and 18 % (2 %) in July. The LNO_x plume parameterization allows the transport of the effects on the non-linear chemistry occurring within the plume and the conversion of NO_x to the nitrogen reservoir species (mainly HNO_3). However, the most significant impact is the transport of the LNO_x as a plume. That implies a delay of (i) the NO_x release into the point grid and (ii) ozone production from NO_x emitted by lightning flashes corresponding to the decrease of the NO_x and O_3 mixing ratios at large scale over regions of emissions and their increase over transport pathway.

The sensitivity of the NO_x and O_3 mixing ratios around the mean value depending on the known uncertainties on the plume physics and chemistry key parameters has been estimated. The highest sensitivity is obtained for the continental tropical regions with ΔNO_x [-33.1; $+29.7$] ppt and ΔO_3 [-1.56; $+2.16$] ppb, in January, and ΔNO_x [-14.3; $+21$] ppt and ΔO_3 [-1.18; $+1.93$] ppb, in July. Concerning the β_1 and β_2 fractions, the highest sensitivity depending on the fraction uncertainties for NO_x is $\Delta NO_x[-2.3; +0.9] \cdot 10^{-2}$ ppt over the continental tropical regions, and ΔO_3 $[-10; +11] \cdot 10^{-4}$ ppb for O_3 over the tropical ocean in January. In summer, the maximum ranges are calculated over oceans in the mid-latitudes for NO_x such as $\Delta NO_x[-21.1; +6.6] \cdot 10^{-2}$ ppt and in the tropics for O_3 with ΔO_3 $[-30; -2] \cdot 10^{-4}$ ppb. Accordingly, parameters leading to the highest uncertainties on results and which drive the plume-in-grid parameterization are NO_i and D_h.

This study demonstrates the importance to consider the plume-in-grid chemistry related to the lightning NO_x emissions occurring at smaller scale for global calculations. Taking into account the plume dilution into the background atmosphere in time and space with the transport of the NO_x and O_3 non-linear chemistry effects and the conversion of NO_x into HNO_3 reservoir species, implies more realistic NO_x and O_3 concentrations in CTM. The plume-in-grid approach, by allowing a more realistic sub-grid chemistry will allow improving the different steps in the lightning NO_x

emissions modeling such as the convection process, the calculation of the NO molecules produced by lightning discharges depending on regions according to recent and future satellite observations, and also processes like the HNO_3 scavenging and the HNO_3 uptake by ice crystals.

Acknowledgements. The GEOS-Chem community (Harvard University) and the Laboratoire d'Aŕologie (UPS / CNRS) supported this work. The authors acknowledge for the help of Lee T. Murray (NASA, NY, USA) for his expertise on the lightning NO_x emissions module in the GEOS-Chem model. We thank the University Paul Sabatier III of Toulouse for giving the ATUPS grant allowing the collaboration with the Wolfson Atmospheric Chemistry Laboratories of York in the research group of Mathew J. Evans.

References

Amos, H. M., Jacob, D. J., Holmes, C. D., Fisher, J. A., Wang, Q., and co authors: Gas-particle partitioning of atmospheric Hg(II) and its effect on global mercury deposition, Atmospheric Chemistry and Physics, 12, 591–603, 2012.

Aumont, B.: Modélisation de la chimie troposphérique, Val de Marne, 2005.

Banerjee, A., Archibald, A. T., Maycock, A. C., Telford, P., Abraham, N. L., and co authors: Lightning NOx, a key chemistry-climate interaction: impacts of future climate change and consequences for tropospheric oxidising capacity, Atmospheric Chemistry and Physics, 14, 9871–9881, 2014.

Bechtold, P., Bazile, E., Guichard, F., Mascart, P., and Richard, E.: A mass-flux convection scheme for regional and global models, Q. J. R. Meteorol. Soc., 127, 869–886, 2000.

Bey, I., Jacob, D. J., Yantosca, R. M., Logan, J. A., Field, B. D., Fiore, A. M., Li, Q., Liu, H. Y., Mickley, L. J., and Schultz, M. G.: Global modeling of tropospheric chemistry with assimilated meteorology: model description and evaluation, Journal of Geophysical Reasearch, 106, 23,073–23,095, 2001.

Bian, H. and Prather, M. J.: Fast-J2: Accurate simulation of stratospheric photolysis in global chemical models, Journal of Atmospheric Chemistry, 41, 281–296, 2002.

Cariolle, D., Caro, D., Paoli, R., Hauglustaine, D. A., Cuénot, B., Cozic, A., and Paugam, R.: Parametrization of plume chemistry into large-scale atmospheric models: application to aicraft NOx emissions, Journal of Geophysical Reasearch, 114, 2009.

Choi, Y., kim, J., Eldering, A., Osterman, G., Yung, Y. L., Gu, Y., and Liou, K. N.: Lightning and anthropogenic NOx sources over the United States and the western North Atlantic Ocean: impact on OLR and radiative effects, Geophysical Research Letters, 36, 2009.

Christian, H. J., Blakeslee, R. J., Boccippio, D. J., Boeck, W. L., and et al., D. E. B.: Global frequency and distribution of lightning as observed from space by the Optical Transient Detector, Journal of Geophysical Reasearch, 108, 4005, 2003.

Cohard, J.-M. and Pinty, J. P.: A comprehensive two-moment warm microphysical bulk scheme. I: Description and tests, Q. J. R. Meteorol. Soc., 126, 1815–1842, 2000.

Cooper, M., Martin, R. V., Wespes, C., Coheur, P.-F., Clerbaux, C., and co authors: Tropospheric nitric acid columns from the IASI satellite instrument interpreted with a chemical transport model: implications for parameterizations of nitric oxide production by lightning, Journal of Geophysical Reasearch, 119, 10,068–10,079, 2014.

Cuxart, J., Bougeault, P., and Redelsperger, J. L.: A turbulence scheme allowing for mesoscale and large-eddy simulations, Q. J. R. Meteorol. Soc., 126, 1–30, 1999.

Damian, V., Sandu, A., Damian, M., Potra, F., and Camichael, G. R.: The kinetic preprocessor KPP - a software environment for solving chemical kinectics, Computers and Chemical Engineering, 26, 1567–1579, 2002.

Dye, J. E., Ridley, B. A., Skamarock, W., Barth, M., and Venticinque, M.: An overview of the Stratospheric-Tropospheric experiment: radiation, aerosols, and ozone (STERAO)-Deep convection experiment with results for the July 10, 1996 storm, Journal of Geophysical Reasearch, 105, 10,023–10,045, 2000.

Emmerson, K. M. and Evans, M. J.: Comparison of tropospheric gas-phase chemistry schemes for use within global models, Atmospheric Chemistry and Physics, 9, 1831–1845, 2009.

Evans, M. J. and Jacob, D. J.: Impact of new laboratory studies of N2O5 hydrolysis on global model budgets of tropospheric nitrogen oxides, ozone, and OH, Geophysical Research Letters, 32, 2005.

Franzblau, E.: Electrical discharges involving the formation of NO, NO2, HNO3 and O3, Journal of Geophysical Reasearch, 96, 22,337–22,345, 1991.

Gregory, D., Morcrette, J.-J., C., J., Beljaars, A. C. M., and Stockdale, T.: Revision of convection, radiation and cloud schemes in the ECMWF Integrated Forecasting System, Q. J. R. Meteorol. Soc., 126, 1685–1710, 2000.

Grewe, V.: Impact of climate variability on tropospheric ozone, Science of the Total Environment, 374, 167–181, 2007.

Guenther, A. B., Jiang, X., Heald, C. L., Sakulyanontvittaya, T., and D, T.: The model of emissions of gases and aerosols from nature version 2.1 (MEGAN2.1): an extended and updated framework for modeling biogenic emissions, Geoscientific Model Development, 5, 1471–1492, 2012.

Hauglustaine, D., Emmons, L., Newchurch, M., Brasseur, G., Takao, T., Matsubara, K., Johnson, J., Ridley, B., Stith, J., and Dye, J.: On the role of lightning NOx in the formation of tropospheric ozone plumes: a global model perspective, Journal of Atmospheric Chemistry, 38, 277–294, 2001.

Hauglustaine, D. A., Granier, C., and Brasseur, G. P.: Impact of present aircraft emissions of nitrogen oxides on troposheric ozone and climate forcing, Geophysical Research Letters, 21, 2031–2034, 1994.

Hudman, R. C., Jacob, D. J., Turquety, S., Leibensperger, E. M., Murray, L. T., and al.: Surface and lightning sources of nitrogen oxides over the United States: Magnitudes, chemical evolution, and outflow, Journal of Geophysical Reasearch, 112, 2007.

Huntrieser, H., Schlager, H., Feigl, C., and Höller, H.: Transport and production of NOx in electrified thunderstorms: survey of previous studies and new observations at midlatitudes, Journal of Geophysical Reasearch, 103, 28,247–28,264, 1998.

Huntrieser, H., Feigl, C., Schlager, H., Schröder, F., Gerbig, C., and van Velthoven, P.: Airborne measurements of NOx, tracer species, and small particles during the European Lightning Nitrogen Oxides Experiment, Journal of Geophysical Reasearch, 107, 4113, 2002.

Huszar, P., Cariolle, D., Paoli, R., Halenka, T., Belda, M., and al.: Modeling the regional impact of ship emissions on NOx and ozone levels over the Eastern Atlantic and Western Europe using ship plume parameterization, Atmospheric Chemistry and Physics, 10, 6645–6660, 2010.

Jacobson, M. Z. and Turco, R. P.: SMVGEAR: a sparse-matrix, vectorized gear code for atmospheric models, Atmospheric Environment, 28, 273–284, 1994.

Jaéglé, L., Jacob, D. J., Wang, Y., Weinheimer, A. J., Ridley, B. A., and co authors: Soucres and chemistry of NOx in the upper troposphere over the United Sates, Geophysical Research Letters, 25, 1705–1708, 1998.

Jenkin, M. E., Saunders, S. M., and Pilling, M. J.: The tropospheric degradation of volatile organic compounds: a protocol for mechanism development, Atmospheric Environment, 31, 81–104, 1997.

Klemp, J. B. and Wilhelmson, R. B.: The simulation of three-dimensional convective storm dynamics, Journal of Atmospheric Sciences, 35, 1070–1096, 1978.

Knollenberg, R. G.: Measurements of the growth of the ice budget in a persisting contrail, Journal of the Atmospheric Sciences, 29, 1367–1374, 1972.

Knollenberg, R. G., Kelly, K., and Wilson, J. C.: Measurements of high number densities of ice crystals in the tops of tropical cumulonimbus, Journal of Geophysical Reasearch, 98, 8639–8664, 1993.

Labrador, L. J., von Kuhlmann, R., and Lawrence, M. G.: Strong sensitivity of the global mean OH concentration and te tropospheric oxidizing efficiency to the source of NOx from lightning, Geophysical Research Letters, 31, 2004.

Lafore, J. P., Stein, J., Asencio, N., Bougeault, P., Ducrocq, V., Duron, J., Fischer, C., Héreil, P., Mascart, P., Masson, V., Pinty, J. P., Redelsperger, J. L., Richard, E., and de Arellano, J. V.-G.: The meso-NH Atmospheric Simulation System. Part I: adiabatic formulation and control simulations, Ann. Geophysicae, 16, 90–109, 1998.

Lange, L., Hoor, P., Helas, G., Fischer, H., and et al., D. B.: Detection of lightning-produced NO in the mid-latitude upper troposphere during STREAM 1998, Journal of Geophysical Reasearch, 106, 27,777–27,785, 2001.

Lascaux, F., Richard, E., and Pinty, J. P.: Numerical simulations of three different MAP IOPs and the associated microphysical processes, Q. J. R. Meteorol. Soc., 132, 1907–1926, 2006.

Lin, J.-T. and McElroy, M. B.: Impacts of boundary layer mixing on pollutant vertical profiles in the lower troposphere: implications to satellite remote sensing, Atmospheric Environment, 44, 1726–1739, 2010.

Lin, S.-J. and Rood, R. B.: Multidimensional flux-form semi-lagrangian transport scheme, Monthly Weather Review, 124, 2046–2070, 1996.

Lin, X., Trainer, M., and Liu, S. C.: On the nonlinearity of the tropospheric ozone production, Journal of Geophysical Reasearch, 93, 15 879–15 888, 1988.

Liu, H., Jacob, D. J., Rey, I., and Yantosca, R. M.: Constraints from 210Pb and 7Be on wet deposition and transport in a global three-dimensional chemical tracer model driven by assimilated meteorological fields, Journal of Geophysical Reasearch, 106, 12,109–12,128, 2001.

Madronich, S. and Flocke, S.: Environmental Photochemistry, Springer, 1999.

Martin, R. V., Jacob, D. J., Logan, J. A., Bey, I., Yantosca, R. M., Staudt, A. C., Li, Q., Fiore, A. M., Duncan, B. N., and Liu, H.: Interpretation of TOMS observations of tropical tropospheric ozone with a global model and in situ observations, Journal of Geophysical Reasearch, 107, 4351, 2002.

Martin, R. V., Sauvage, B., Folkins, I., Sioris, C. E., Boone, C., Bernath, P., and Ziemke, J.: Space-based constraints on the production of nitric oxide by lightning, Journal of Geophysical Reasearch, 112, 2007.

Monks, P. S.: Gas-phase radical chemistry in the tropopshere, Chemical Society Revews, 34, 376–395, 2005.

Moorthi, S. and Suarez, M. J.: Relaxed Arakawa-Schubert: a parameterization of moist convection for general circulation models, Monthly Weather Review, 120, 978–1002, 1991.

Murray, L. T., Jacob, D. J., Logan, J. A., Hudman, R. C., and Koshak, J.: Optimized regional and interannual variability of lightning in a global chemical transport model constrained by LIS/OTD satelite data, Journal of Geophysical Reasearch, 117, 2012.

Olivier, J. G. J.: Recent trends in global greenhouse gas emissions: regional trends and spatial distribution of key sources, Environment Sciences, 2, 81–89, 2005.

Ott, L. E., Pickering, K. E., Stenchikov, G. L., Allen, D. J., DeCaria, A. J., and co authors: Production of lightning NOx and its vertical distribution calculated from three-dimensional cloud-scale chemical transport model simulations, Journal of Geophysical Reasearch, 115, 2010.

Paoli, R., Cariolle, D., and Sausen, R.: Review of effective emissions modeling and computation, Geoscientific Model Development, 4, 643–667, 2011.

Pickering, K. E., Thompson, A. M., Dickerson, R. R., Luke, W. T., MacNamara, D. P., Greenberg, J. P., and Zimmerman, P. R.: Model calculations of tropospheric ozone production potentiel following observed convective events, Journal of Geophysical Reasearch, 95, 14,049–14,062, 1990.

Pinty, J. P. and Jabouille, P.: A mixed-phase cloud parameterization for use in a mesoscale non-hydrostatic model: simulations of a squall line and of orographic precipitation, American Meteorological Society, pp. 217–220, 1999.

Price, C. and Rind, D.: A simple lightning parameterization for calculating global lightning distributions, Journal of Geophysical Reasearch, 97, 9919–9933, 1992.

Price, C. and Rind, D.: Possible implications of global climate change on global lightning distributions and frequencies, Journal of Geophysical Reasearch, 99, 10,823–10,831, 1994.

Sander, S. P., Friedl, R. R., Golden, D. M., Kurylo, M. J. M., and et al., G. K. M.: Chemical kinetics and photochemical data for use in atmosperic studies, evaluation number 15, Tech. rep., NASA, 2006.

Saunders, S. M., Jenkin, M. E., Derwent, R. G., and Pilling, M. J.: Protocol for the development of the Master Chemical Mechanism, MCM v3 (Part A): tropospheric degradation of non-aromatic volatile organic compounds, Atmospheric Chemistry and Physics, 3, 161–180, 2003.

Sauvage, B., Martin, R. V., van Donkelaa, A., and Ziemke, J. R.: Quantification of the factors controlling tropical tropopsheric ozone and the South Atlantic maximum, Journal of Geophysical Reasearch, 112, 2007a.

Sauvage, B., Martin, R. V., van Donkelaar, A., Liu, X., Chance, K., Jaeglé, L., Palmer, P. I., Wu, S., and Fu, T. M.: Remote sensed and in situ constraints on processes affecting tropical tropospheric ozone, Atmospheric Chemistry and Physics, 7, 815–838, 2007b.

Schumann, U. and Huntrieser, H.: The global lightning-induced nitrogen oxides source, Atmospheric Chemistry and Physics, 7, 3823–3907, 2007.

Stark, M. S., Harrison, J. T. H., and Anastasi, C.: Formation of nitrogen oxides by electrical discharges and implications for atmospheric lightning, Journal of Geophysical Reasearch, 101, 6963–6969, 1996.

Stith, J., Dye, J., Ridley, B., Laroche, P., Defer, E., Hübler, G., Zerr, R., and Venticinque, M.: NO signatures from lightning flashes, Journal of Geophysical Reasearch, 104, 16,081–16,089, 1999.

Stockwell, D. Z., Giannakopoulos, C., Plantevin, P. H., Carver, G. D., Chipperfield, M. P., Law, K. S., Pyle, J. A., Shallcross, D. E., and Wang, K. Y.: Modelling NOx from lightning and its impact on global chemical fields, Atmospheric Environment, 33, 4477–4493, 1999.

Streets, D. G., Zhang, Q., Wang, L., He, K., Hao, J., and al.: Revisting China's CO emissions after the Transport and Chemical evolution over the Pacific (TRACE-P) mission: Synthesis of inventories, atmospheric modeling, and observations, Journal of Geophysical Reasearch, 111, 2006.

Teyssèdre, H., Michou, M., Clark, H. L., Josse, B., Karcher, F., Olivié, D., Peuch, V.-H., Saint-Martin, D., Cariolle, D., Attié, J.-L., Nédélec, P., Ricaud, P., Thouret, V., van der A, R. J., Volz-Thomas, A., and Cheroux, F.: A new tropospheric ans stratospheric chemistry and transport model MOCAGE-Climat for multi-year studies: evaluation of the present-day climatology and sensitivity to surface processes, Atmospheric Chemistry and Physics, 7, 5815–5860, 2007.

Tost, H., Jöckel, P., and Lelieveld, J.: Lightning and convection parameterisations - uncertainties in global modelling, Atmospheric Chemistry and Physics, 7, 4553–4568, 2007.

Trier, S. B. and Sharman, R. D.: Convection-permitting simulations of the environment supporting widespread turbulence within the upper-level outflow of a mesoscale convective system, American Meteorological Society, 137, 1972–1990, 2008.

Tulet, P., Crassier, V., Solmon, F., Guedalia, D., and Rosset, R.: Description of the Mesoscale Nonhydrostatic chemistry model and application to a transboundary pollution episode between northern France and southern England, Journal of Geophysical Reasearch, 108, 4021, 2003.

Tulet, P., Grini, A., Griffin, R. J., and Petitcol, S.: ORILAM-SOA: A compitationnaly efficient model for predicting secondary organic aerosols in three-dimensional atmospheric models, Journal of Geophysical Reasearch, 111, 2006.

van der Werf, G. R., Randerson, J. T., Giglio, L., G. J. Collatz, M. M., Kasibhatla, P. S., Morton, D. C., DeFries, R. S., Jin, Y., and van Leeuwen, T. T.: Global fire emissions and the contribution of deforestation, savanna, forest, agricultural, and peat fires (1997-2009), Atmospheric Chemistry and Physics, 10, 11 707–11 735, 2010.

Wang, Q., Jacob, D. J., Fisher, J. A., Mao, J., Leibensperger, E. M., and co authors: Sources of carbonaceous aerosols and deposited black carbon in the Arctic in winter-spring: implications for radiative forcing, Atmospheric Chemistry and Physics, 11, 12 453–12 473, 2011.

Wang, Y., Jacob, D. J., and Logan, J. A.: Global simulation of tropospheric O3-NOx-hydrocarbon chemistry - 1. Model formulation, Journal of Geophysical Reasearch, 103, 10,713–10,725, 1998.

Wennberg, P. O., Hanisco, T. F., Jaeglé, L., Jacob, D. J., Hinsta, E. J., Lanzendorf, E. J., Anderson, J. G., Gao, R. S., and al.: Hydrogen radicals, nitrogen radicals and the production of O3 in the upper troposphere, Science, 279, 1998.

Wesely, M. L.: Parameterization of surface resistances to gaseous dry deposition in regional-scale numerical models, Atmospheric Environment, 23, 1293–1304, 1989.

WMO: Scientific Assessment of Ozone Depletion: 1998, Tech. rep., World Meteorological Organization, 1999.

Yevich, R. and Logan, J. A.: An assessment of biofuel use and burning of agricultural waste in the developing world, Global Biogeochemical Cycles, 17, 1095, 2003.

Yienger, J. J. and Levy, H.: Empirical model of global soil-biogenic NOx emissions, Journal of Geophysical Reasearch, 100, 11,447–11,464, 1995.

Zhang, Q., Streets, D. G., G. R. Carmichael, K. B. H., Huo, H., and al.: Asian emissions in 2006 for the NASA INTEX-B mission, Atmospheric Chemistry and Physics, 9, 5131–5153, 2009.

Zhang, R., Tie, X., and Bond, D. W.: Impacts of anthropogenic and natural NOx sources over the U.S. on tropospheric chemistry, Proceedings of the National Academy of Sciences of the United States of America, 100, 1505–1509, 2003.

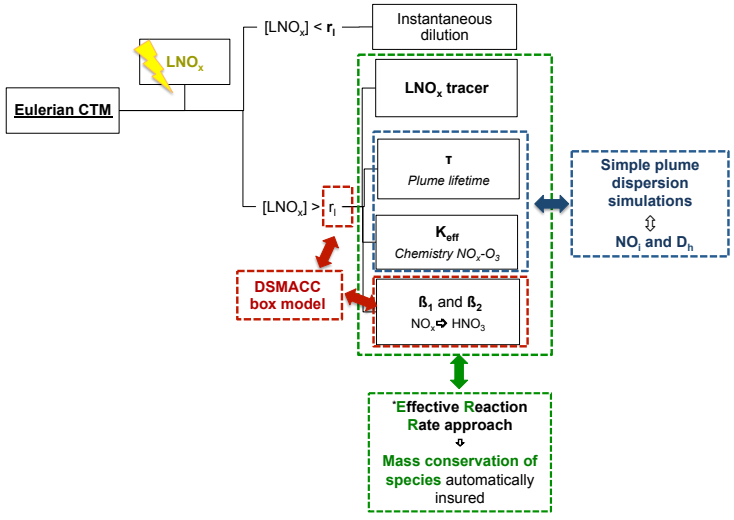

Figure 1. Diagram of the lightning NO_x plume parameterization based on the Effective Reaction Rate approach. The arrows link the parameters to their estimate approach. The red boxes are for the parameters estimated with the DSMACC model and the blue boxes are related to the parameters calculated with the simple plume dispersion model. Finally the green boxes show the Effective Reaction Rate approach in the GEOS-Chem CTM.

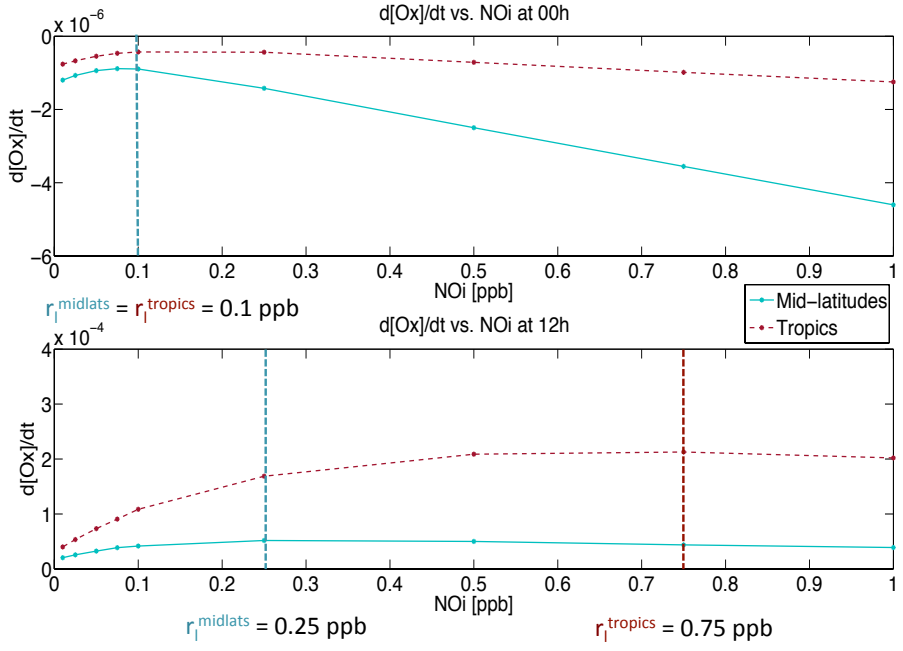

Figure 2. r_l critical value and odd oxygen trends from DSMACC chemistry box model simulations for mid-latitudes (solid line) and tropics (dotted line) (a) at midnight (upper panel) and (b) at midday (bottom panel).

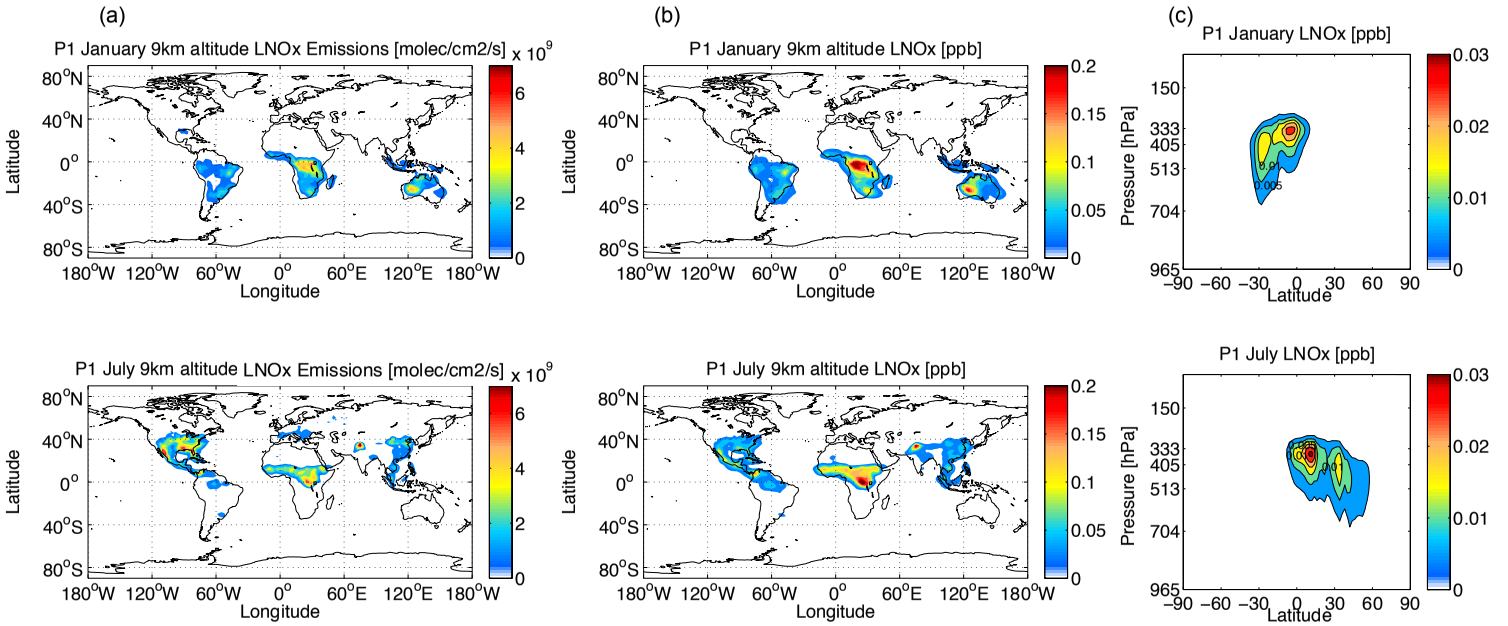

Figure 3. (left panels, a) Geographical distributions at 9 km altitude of lightning NO_x emissions, (middle panels, b) the geographical distributions of the related LNO_x tracer (in ppb) and (right panels, c) the zonal averaged of the LNO_x tracer (in ppb), for January (top) and July (bottom). Experiment $P1$, using τ and K_{eff} determined with $D_h = 15\ m^2 \cdot s^{-1}$ and NO_i^{mean}, performed with the GEOS-Chem model.

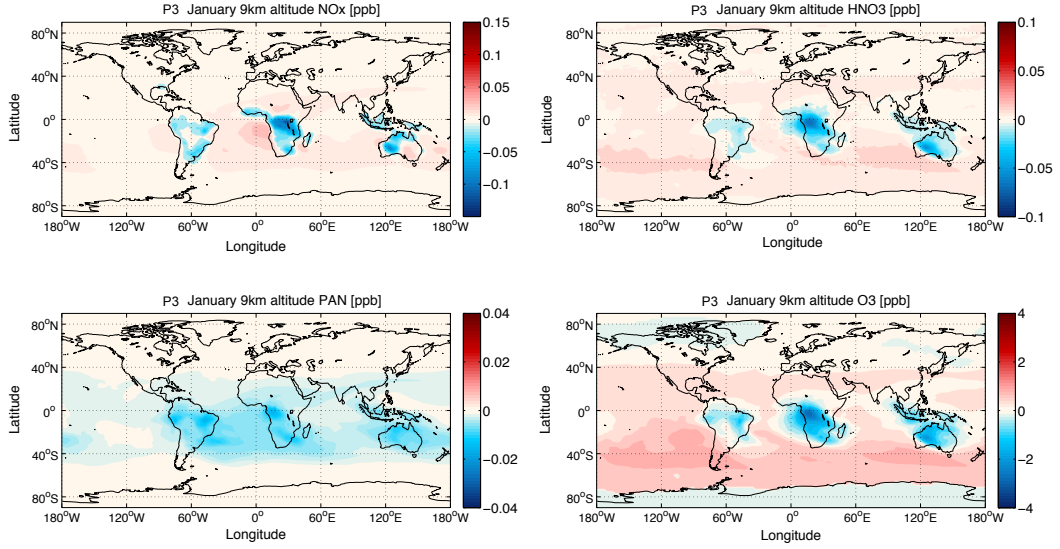

Figure 4. Geographical distributions of NO_x, HNO_3, PAN, and O_3 variations (in ppb) at 9 km altitude for January from the absolute difference ($P3$) between $P1$ and BC experiments. $P1$ was performed using τ and K_{eff} determined with $D_h = 15\ m^2 \cdot s^{-1}$ and NO_i^{mean} with GEOS-Chem.

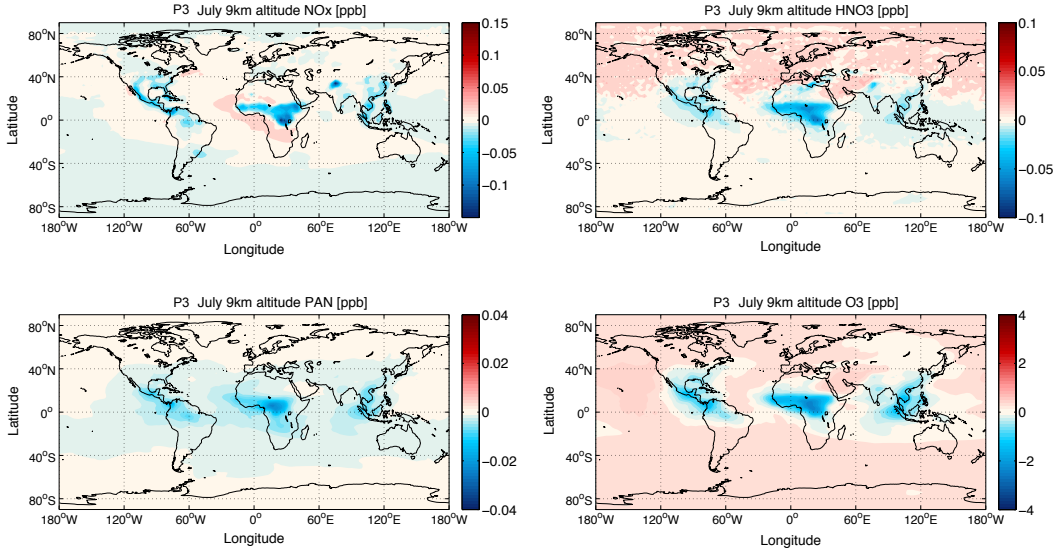

Figure 5. Geographical distributions of NO_x, HNO_3, PAN, and O_3 variations (in ppb) at 9 km altitude for July from the absolute difference ($P3$) between $P1$ and BC experiments. $P1$ was performed using τ and K_{eff} determined with $D_h = 15\ m^2 \cdot s^{-1}$ and NO_i^{mean} with GEOS-Chem.

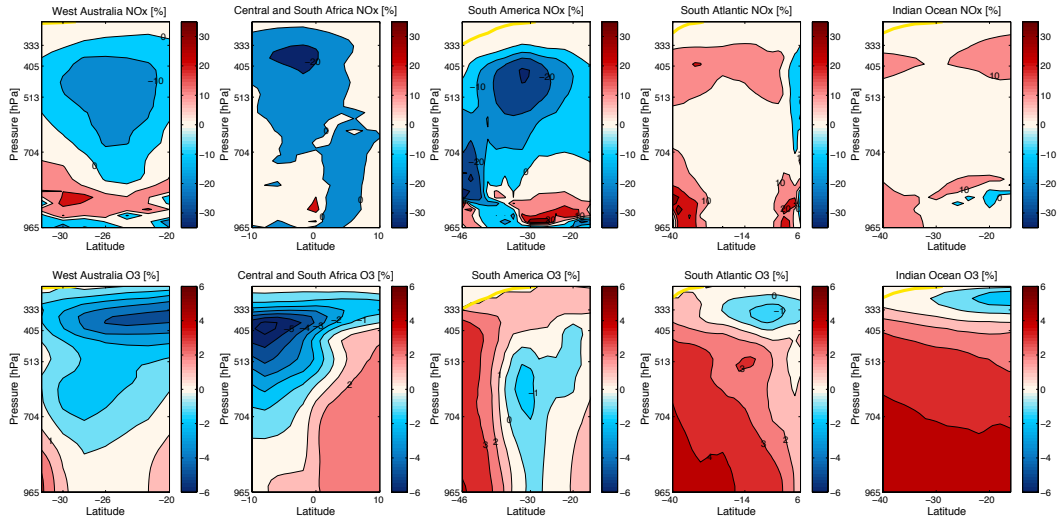

Figure 6. Zonal averaged NO_x (upper panels) and O_3 (bottom panels) variations (in %) over the regions characterized by strong NO_x emissions for January (the yellow solid line represents the tropopause level), from the relative difference between $P1$ and BC experiments ($P3/BC$). $P1$ was performed using τ and K_{eff} determined with $D_h = 15\ m^2 \cdot s^{-1}$ and NO_i^{mean} with GEOS-Chem.

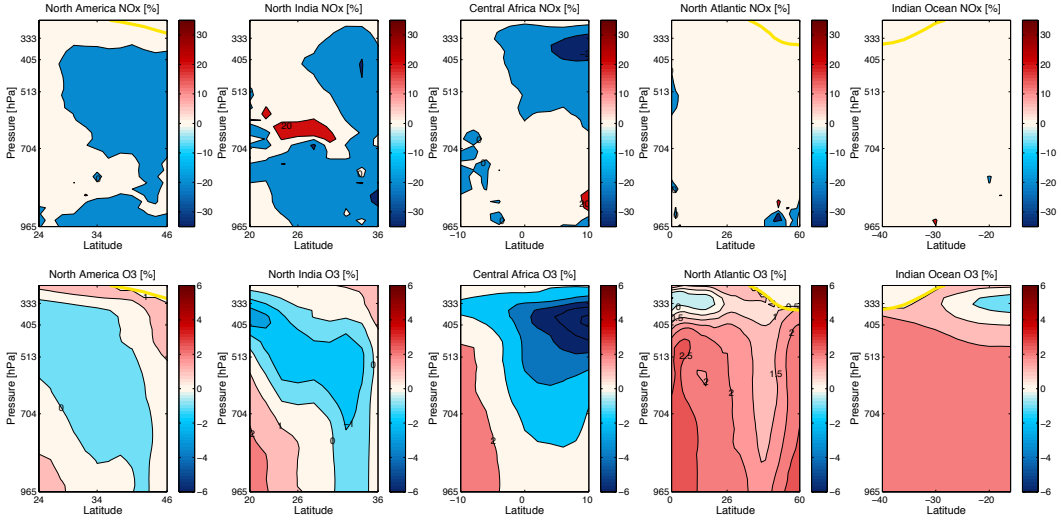

Figure 7. Zonal averaged NO_x (upper panels) and O_3 (bottom panels) variations (in %) over the regions characterized by strong NO_x emissions for July (the yellow solid line represents the tropopause level), from the relative difference between $P1$ and BC experiments ($P3/BC$). $P1$ was performed using τ and K_{eff} determined with $D_h = 15\ m^2 \cdot s^{-1}$ and NO_i^{mean} with GEOS-Chem.

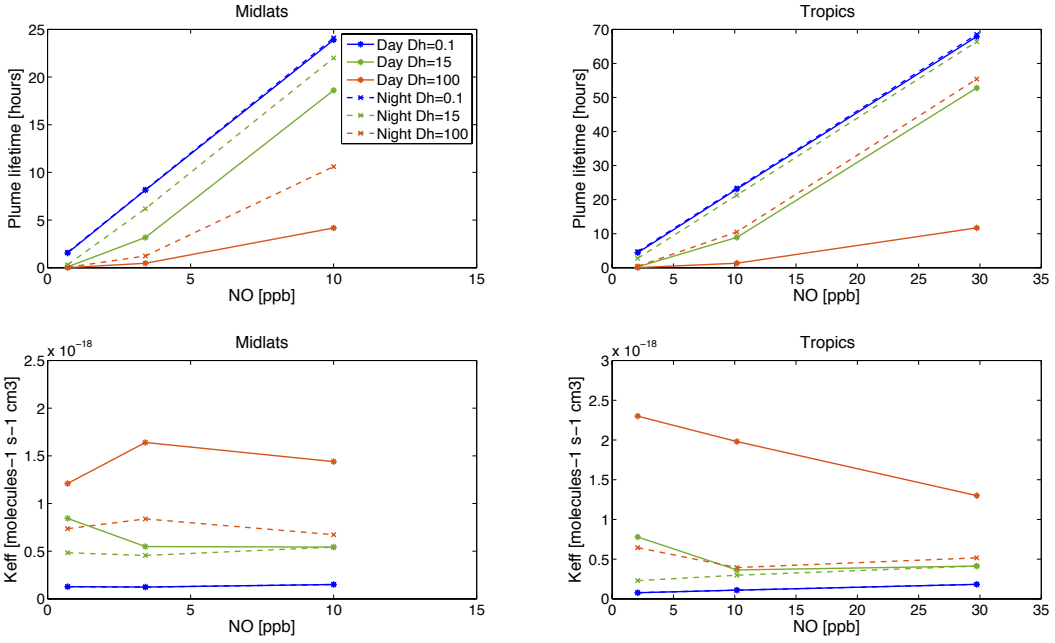

Figure 8. The plume lifetime (τ, upper panels) and the effective reaction rate constant (K_{eff}, bottom panels) depending (i) on the horizontal coefficient diffusion (D_h, $m^2 \cdot s^{-1}$) for the mid-latitudes (left panels) and the tropics (right panels) and (ii) on the NO mixing ratio injected by lightning (NO_i, in ppb).

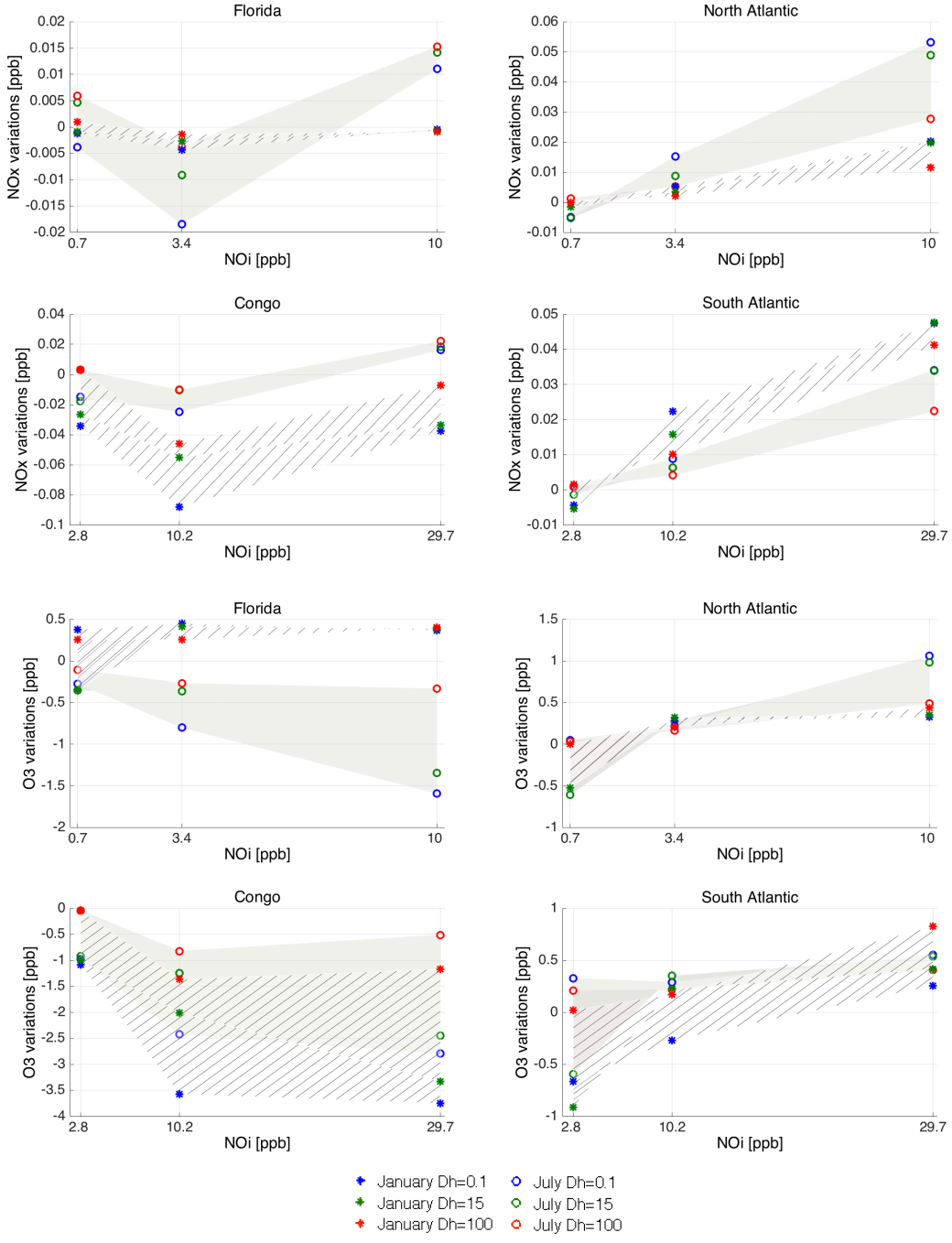

Figure 9. The NO_x (a) and O_3 (b) sensitivity at 9 km altitude depending on the horizontal coefficient diffusion (D_h, $m^2 \cdot s^{-1}$) and on the NO mixing ratio injected by lightning (NO_i, ppb) for the mid-latitudes (Florida and North Atlantic) and the tropics (Congo and South Atlantic). Intervals are hatched in January and filled in grey in July. Markers correspond to the NO_x variations simulated for $D_h = 0.1\ m^2 \cdot s^{-1}$ (red ones), $D_h = 15\ m^2 \cdot s^{-1}$ (blue ones) and $D_h = 100\ m^2 \cdot s^{-1}$ (green ones).

	TEMP	PRESS	O_3	NO	NO_2	HNO_3	HNO_4	PAN	N_2O_5	CO
Units	(K)	(hPa)	(ppb)	(ppb)	(ppb)	(ppb)	(ppb)	(ppb)	(ppt)	(ppb)
Mid-latitudes	228	313	67	0.04	0.01	0.15	0.02	0.1	2	94
Tropics	240	313	26	0.03	0.003	0.02	0.006	0.03	2.3	93

	OH	HO_2	H_2O_2	CH_2O	CH_4O_2	C_3H_8	C_5H_8	C_2H_4O	C_3H_6O
Units	(ppb)	(ppt)	(ppt)	(ppb)	(ppb)	(ppb)	(ppb)	(ppb)	(ppb)
Mid-latitudes	0.2	4	0.4	0.06	0.1	0.47	0	7.5	4
Tropics	0.06	6	0.34	0.03	0.17	0.13	7.5	7.5	4

Table 1. The initial atmospheric parameters and background concentrations of chemical species from GEOS-Chem outputs for the DSMACC chemical box model simulations.

Day						
τ (hours)	**Mid-latitudes**			**Tropics**		
NO_i (ppb)	0.7	3.4	10	2.8	10	29.7
$D_h = 0.1$ $(m^2 \cdot s^{-1})$	1.55	8.14	23.9	4.40	23.1	67.9
$D_h = 15$ $(m^2 \cdot s^{-1})$	0.1	3.17	18.6	0.27	8.90	52.8
$D_h = 100$ $(m^2 \cdot s^{-1})$	0.01	0.47	4.17	0.04	1.32	11.7

Night						
τ (hours)	**Mid-latitudes**			**Tropics**		
NO_i (ppb)	0.7	3.4	10	2.8	10	29.7
$D_h = 0.1$ $(m^2 \cdot s^{-1})$	1.62	8.19	24.1	4.74	23.4	68.5
$D_h = 15$ $(m^2 \cdot s^{-1})$	0.31	6.19	22	2.77	21.3	66.4
$D_h = 100$ $(m^2 \cdot s^{-1})$	0.05	1.23	10.6	0.43	10.5	55.4

Table 2. The plume lifetime τ (hours) calculated for mid-latitudes and tropics depending on the initial NO mixing ratio injected by lightning emissions (NO_i, ppb) and the horizontal diffusion coefficient (D_h, $m^2 \cdot s^{-1}$) for day (upper table) and night conditions (bottom table).

Day						
$K_{eff}(10^{-19}\ molecules^{-1}\cdot s^{-1}\cdot cm^3)$	**Mid-latitudes**			**Tropics**		
$NO_i\ (ppb)$	0.7	3.4	10	2.8	10	29.7
$D_h = 0.1\ (m^2\cdot s^{-1})$	1.28	1.24	1.51	0.77	1.2	1.83
$D_h = 15\ (m^2\cdot s^{-1})$	8.44	5.49	5.43	7.79	3.64	4.13
$D_h = 100\ (m^2\cdot s^{-1})$	12.1	16.4	14.4	23	19.8	13

Night						
$K_{eff}(10^{-19}\ molecules^{-1}\cdot s^{-1}\cdot cm^3)$	**Mid-latitudes**			**Tropics**		
$NO_i\ (ppb)$	0.7	3.4	10	2.8	10	29.7
$D_h = 0.1\ (m^2\cdot s^{-1})$	1.28	1.24	1.51	0.77	1.10	1.83
$D_h = 15\ (m^2\cdot s^{-1})$	4.84	4.55	5.43	2.3	2.98	4.13
$D_h = 100\ (m^2\cdot s^{-1})$	7.36	8.39	6.73	6.45	3.94	5.16

Table 3. The effective reaction rate constant K_{eff} ($10^{-19}\ molecules^{-1}\cdot s^{-1}\cdot cm^3$) in mid-latitudes and tropics depending on the initial NO mixing ratio injected by lightning emissions (NO_i, ppb) and the horizontal diffusion coefficient (D_h, $m^2\cdot s^{-1}$) for day (upper table) and night conditions (bottom table).

Day						
β_1 (10^{-4})	**Mid-latitudes**			**Tropics**		
NO_i (ppb)	0.7	3.4	10	2.8	10	29.7
Aerosols	2.53	3.34	3.45	2.51	2.95	2.6
Ice	0.23	0.3	0.3	0.2	0.23	0.3
Mean	1.38	1.8	1.88	1.34	1.59	1.47

Night						
β_2 (10^{-3})	**Mid-latitudes**			**Tropics**		
NO_i (ppb)	0.7	3.4	10	2.8	10	29.7
Aerosols	14.3	9.89	8	4.9	1.69	0.24
Ice	14.4	9.96	8.06	4.89	1.70	0.24
Mean	14.4	9.92	8.03	4.88	1.7	0.24

Table 4. The fractions of NO_x conversion into HNO_3 within the plume (β_1 and β_2) in mid-latitudes and tropics depending on the initial NO mixing ratio injected by lightning emissions (NO_i, ppb) and on particles for day (upper table) and night conditions (bottom table).

Parameters	**Experiments**											
	P1									**P2**		
D_h $(m^2 \cdot s^{-1})$	0.1			15			100			15		
NO_i (ppb)	Min	Mean	Max	Min	Mean	Max	Min	Mean	Max	Mean		
Mid-latitudes	0.7	3.4	10	0.7	3.4	10	0.7	3.4	10	3.4		
Tropics	2.8	10.2	29.7	2.8	10.2	29.7	2.8	10.2	29.7	10.2		
β_1	Mean									0	Min	$Mean$ Max
β_2	Mean									0	Min	$Mean$ Max

Table 5. Values of the parameters for the plume parameterization corresponding to the experiments $P1$ and $P2$.

	JANUARY				JULY			
	Mid-latitudes		**Tropics**		**Mid-latitudes**		**Tropics**	
	Florida	North Atlantic	Congo	South Atlantic	Florida	North Atlantic	Congo	South Atlantic
$\Delta NO_x \pm$	$[-1.7; +1.8]$	$[-8.2; +1.7]$	$[-33.1; +29.7]$	$[-6.5; +6.9]$	$[-9.3; +5.4]$	$[-21.1; +6.6]$	$[-14.3; +21]$	$[-11.5; +2.6]$
$\Delta O_3 \pm$	$[-0.16; +0.72]$	$[-0.12; +0.53]$	$[-1.56; +2.16]$	$[-0.49; +0.94]$	$[-0.44; +1.01]$	$[-0.49; +0.66]$	$[-1.18; +1.93]$	$[-0.14; +0.92]$

Table 6. The sensitivity of NO_x (in ppt) and O_3 (in ppb) depending on the horizontal diffusion coefficient (D_h, $m^2 \cdot s^{-1}$) and on the NO_i mixing ratio (ppb) injected by lightning for mid-latitudes (Florida and North Atlantic) and tropics (Congo and South Atlantic) in January and July.

	JANUARY				JULY			
	Mid-latitudes		Tropics		Mid-latitudes		Tropics	
	Florida	North Atlantic	Congo	South Atlantic	Florida	North Atlantic	Congo	South Atlantic
$\Delta NO_x \pm \cdot 10^{-2}$	$[-1.6; -0.06]$	$[-2.3; -2.3]$	$[-2.3; +0.9]$	$[+0.3; +0.6]$	$[-3.3; +1.4]$	$[-21.1; +6.6]$	$[+0.4; +2.1]$	$[-0.9; -0.4]$
$\Delta O_3 \pm \cdot 10^{-4}$	$[-9; +5]$	$[-9; +4]$	$[-3; +22]$	$[-10; +11]$	$[-24; -6]$	$[-6; +19]$	$[-8; +17]$	$[-30; -2]$

Table 7. The sensitivity of NO_x (in ppt) and O_3 (in ppb) depending on β_1 and β_2 values for mid-latitudes (Florida and North Atlantic) and tropics (Congo and South Atlantic) in January and July. Experiment $P1$, using $D_h = 15\ m^2 \cdot s^{-1}$ and NO_i^{mean}, performed with the GEOS-Chem model.